Mendes, J. and Toll, D.G. (2016) *Influence of initial water content on the mechanical behaviour of an unsaturated sandy clay soil,* International Journal of Geomechanics 16(6). http://dx.doi.org/10.1061/(ASCE)GM.1943-5622.0000594.

Influence of initial water content on the mechanical behaviour of an unsaturated sandy clay soil

Mendes J.

joaopaulo.duarte@univ-pau.fr

Université de Pau et des Pays de l'Adour, Pau, France

Formerly Durham University

Toll D. G.

d.g.toll@durham.ac.uk

Durham University, Durham, United Kingdom

Abstract

The mechanical behaviour of a sandy clay soil has been investigated by a series of constant water content triaxial tests on unsaturated samples with suction measurements. The tests were carried out in double cell triaxial cells on compacted samples, and also on samples wetted and dried from the as-compacted conditions. A series of tests on saturated samples was also performed to provide a reference state for the unsaturated tests. Since specimens were at high degrees of saturation (generally greater than 80%), calculations based on effective stress showed a reasonable interpretation of the data for the Critical State parameters M and λ. However, the intercept of the Critical State line in the v axis (Γ) differed, increasing with an increase in water content (at compaction). The data were also analysed using the Bishop stress (p*) approach and a better fitting was achieved in the stress plane where it was possible to define a unique Critical State line, where M was 0.91. However, in the v–p* plane, different critical state lines were still obtained for different compaction water contents. The similarity in the critical state parameters M and λ show that subjecting the soil to wetting and drying paths had little influence on the soil at Critical State conditions, when the pore water pressure changes were taken into account.

1 Introduction

Future climate scenarios for the UK (Jenkins et al., 2010) present concerns for engineers about the performance of earth structures such as embankments that form the transportation network. Intense rainfall and longer drier periods, as are predicted for the UK, may greatly affect the stability of slopes and foundations that are the base of the complex and extended transportation network in the UK. Problems such as shrinkage settlements due to drought and failure of slopes due to intense rainfall are already being experienced to some extent, but are more likely to occur with future climate change.

As the majority of earth structures are built and maintained in unsaturated conditions, to understand the strength changes that can lead to failure of earth structures due to climate change it is necessary to understand the mechanical behaviour of unsaturated soils. The interpretation of the experimental data on unsaturated soils has generated much discussion in literature. The first attempts to explain the engineering behaviour of unsaturated soils used an equivalent effective stress approach (Bishop, 1959) which was expressed as:

$$\sigma' = \sigma - u_a + \chi (u_a - u_w) \quad \text{(Eq. 1)}$$

where σ' is effective stress, σ is total stress, u_w and u_a are pore water pressure and pore air pressure and χ was an empirical factor that varied between 0 and 1 as a function of degree of saturation.

Fredlund et al. (1978) argued that it was better to separate the effects of net stress and suction, rather than combine them into a single "effective stress". Fredlund and Morgenstern (1977) concluded that net normal stress and soil matric suction are the appropriate stress state variables for unsaturated soils. Khalili and Khabbaz (1998) argued for going back to an effective stress approach, proposing that χ could be expressed as a function of suction (related to the air entry value of the soil) rather than degree of saturation. They suggested that expressing χ in this way allowed a unique value of χ to be defined. There have been recent attempts to use a combined stress, often incorporating the degree of saturation, in place of net stress. Jommi (2000) suggested using an average skeleton stress, p^*, as defined in Eq. 2.

$$p^* = p - [S_r.u_w + (1 - S_r).u_a] \quad \text{(Eq. 2)}$$

where p is the mean total stress and S_r is the degree of saturation. This is sometimes referred to as "Bishop stress" as it uses Bishop's equation (Eq. 1) but replaces the empirical parameter χ with the degree of saturation. It does not have to be seen as equivalent to effective stress; it can be used in combination with suction to interpret the behaviour.

Bishop et al. (1960) presented triaxial test data on compacted clay and glacial till (boulder clay). Bishop and Blight (1963) interpreted this data using Bishop's (1959) approach but noted that there were difficulties in interpreting stress-volume change relationships, although they found that the interpretation of the relationship between shear strength and effective stress was less sensitive. Fredlund et al. (1978) presented data from shear box tests on glacial till, Escario & Saez (1986) reported shear strength data on Madrid Grey Clay and Ho and Fredlund (1982) presented triaxial test data on shear strength of two Hong Kong Soils; these sets of data were interpreted in terms of separate stress state variables. Toll (1990) and Toll and Ong (2003) reported data on a compacted clayey gravel and a residual sandy clay respectively; They used a critical state approach, based on separate stress state variables, but where the critical state parameters were expressed as functions of degree of saturation. Wheeler & Sivakumar (1995, 2000) presented triaxial tests on statically compacted specimens of kaolin. They adopted a critical state approach where the parameters were expressed as functions of suction. Tarantino and Tombolato (2005) also reported tests on compacted kaolin, carried out using a shear box fitted with a high suction probe. They attempted to interpret the results using "Bishop stress" but found the fit was not good for suctions up to 2 MPa.

In this paper the study of the mechanical behaviour of the fill material used in the construction of a full scale instrumented embankment constructed in North East England was undertaken as part of a larger investigation of the impacts of climate change on the serviceability and safety of earth structures (embankments) (Hughes et al, 2009). The embankment fill material can be classified as a well graded sandy clay soil of intermediate plasticity.

To determine the mechanical behaviour of the embankment fill material a triaxial testing program was developed, where samples were tested at constant water content (CWC) in unsaturated

conditions. This was the most appropriate form of testing, considering the low permeability of the soil being studied (10^{-10}-10^{-11} m/s) (Hughes et al, 2007). The pore water pressure was continuously monitoring during testing using a high capacity suction probe (capable of direct measurement to suctions of 2MPa) (Lourenço et al., 2006). The triaxial testing program also included a series of saturated consolidated drained triaxial tests, to provide a reference for the testing program on unsaturated samples.

The triaxial testing program was performed on samples compacted at specific water contents being: 15% (the optimum water content, W_{opt}), 20% and 22%. Testing was restricted to this range of water content due to limitations of the suction range of the high capacity suction probe (2 MPa). In order to achieve an insight into the behaviour of samples subject to wetting and drying (due to climate influences), a further series of samples were prepared from the starting water contents (15%, 20% and 22%) that subsequently were wetted or dried after compaction. The wetting and drying was carried out outside the triaxial cells by wetting inside a sealed chamber at high relative humidity or air drying, after which, the samples were placed inside double cell triaxial cells and subjected to constant water content compression and subsequent shearing. Testing was carried out at different confining pressures (50, 150 and 300kPa).

Sets of Critical State parameters, were determined from the triaxial tests for each starting water content, initially using "effective stress" ($p-u_w$) and plotting data in the $v-(p-u_w)$ plane and the $q – (p-u_w)$. The data were also analysed using the average skeleton stress (p^*) approach (Jommi, 2000) ("Bishop stress") as shown in Eq. 2. The effect of the initial (as-compacted) conditions and the subsequent wetting or drying processes were considered in the results.

2 Materials

The fill material from an existing instrumented embankment in the North East of England was chosen for this study. The fill material was single sourced from a stock pile in County Durham (Hughes et al., 2009). The general distribution was found to be 12% of gravel, 16% of sand, 35% of silt and 37% of clay. The Atterberg limits were LL=43.3%, PL=23.7% resulting in a PI=19.6 and LI=-0.05. The material was classified as a well graded sandy clay soil of intermediate plasticity.

From the laboratory compaction curve, shown in Figure 1, it was determined that the maximum dry density and the optimum water content were respectively 1.71Mg/m^3 and 15.5%. Curves are shown for the natural material (unseived) and the same material after sieving through a 2.8mm sieve to remove larger particles. Initial study with the natural fill material had shown large variations in density between similar samples, which were attributed to the presence of the larger particles. Thus, it was decided to sieve the material through a 2.8mm sieve in order to improve sample preparation. The sieved material (which will be referred to as the fill material throughout this manuscript) has the general distribution of 2% gravel, 28% sand, 35% of silt and 35% of clay. The Atterberg limits and classification remained unchanged from the unsieved material.

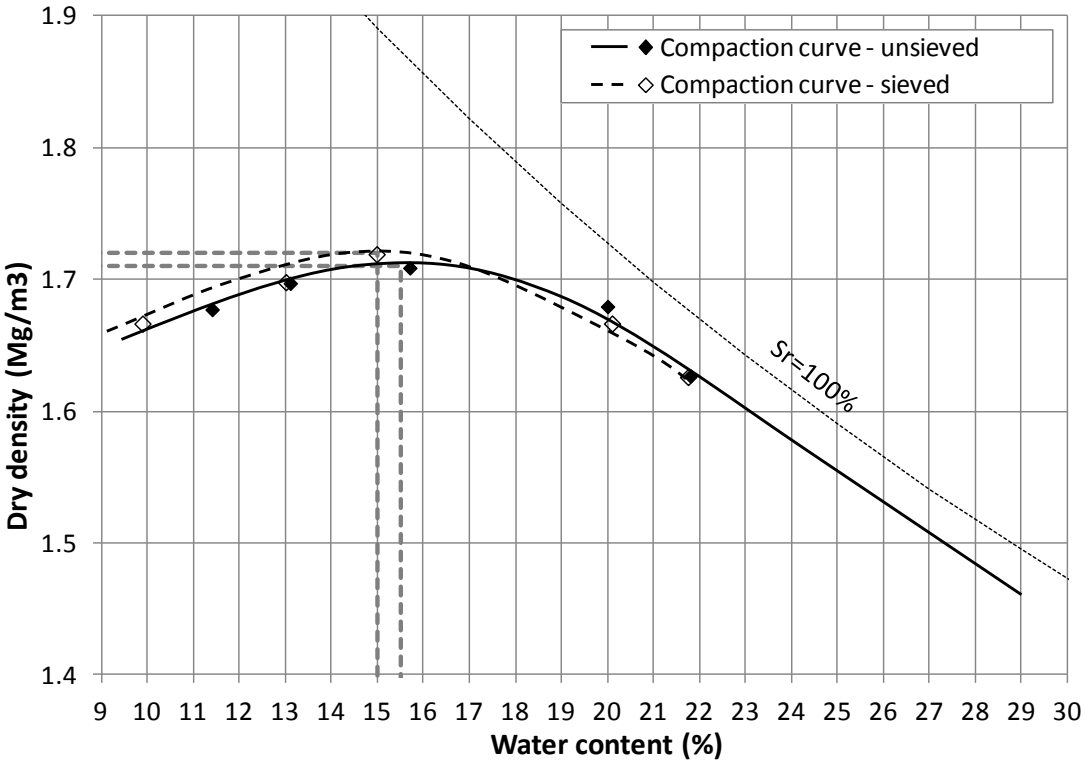

Figure 1 - Compaction curves obtained for unsieved and sieved fill material.

From the compaction curve for the sieved material a lower optimum water content (15%) and a higher maximum dry density (1.72 Mg/m^3) were obtained, see Figure 1, representing only a small shift compared to the curve obtained with the unsieved material.

The soil water retention curve (SWRC) for the unsieved material is show in Figure 2 and 3. The SWRC following a drying path was determined using in-contact Whatman 42 filter papers and high capacity suction probes. The initial water content of the samples, used in the determination of the SWRC, was 25%, which were later air dried in stages to lower water contents. From Figure 3, the apparent air entry value of the soil was estimated to be 550kPa corresponding to 18% of gravimetric water content in Figure 2.

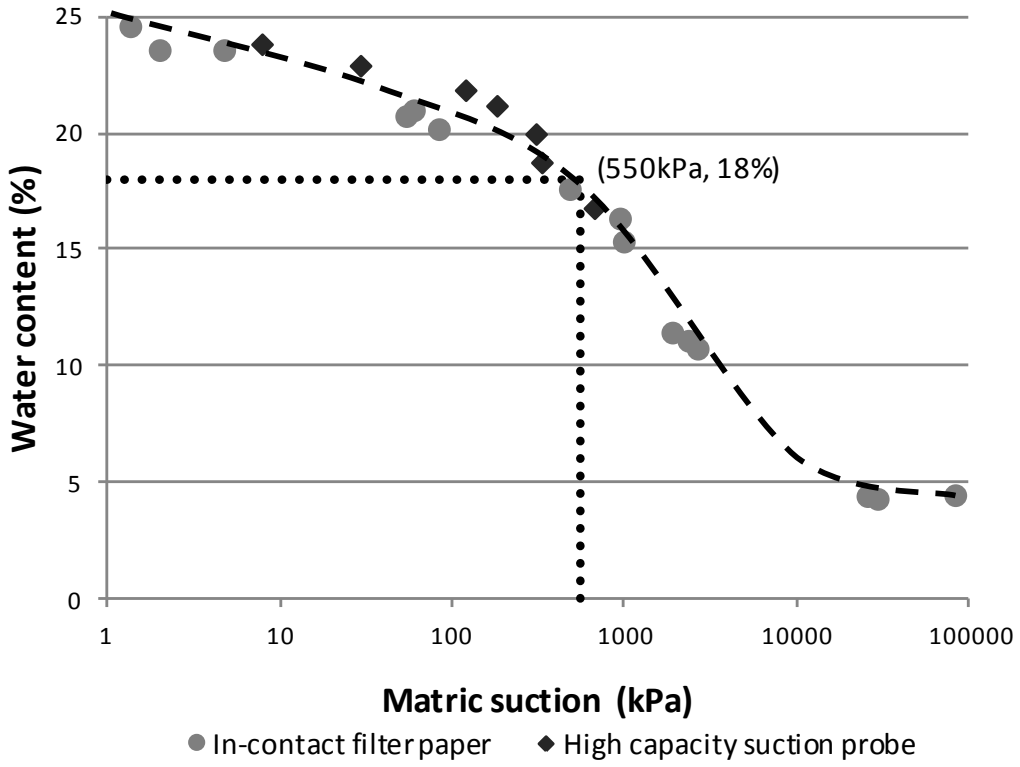

Figure 2 – Gravimetric water content versus matric suction, for compacted samples staged dried from 25% of water content.

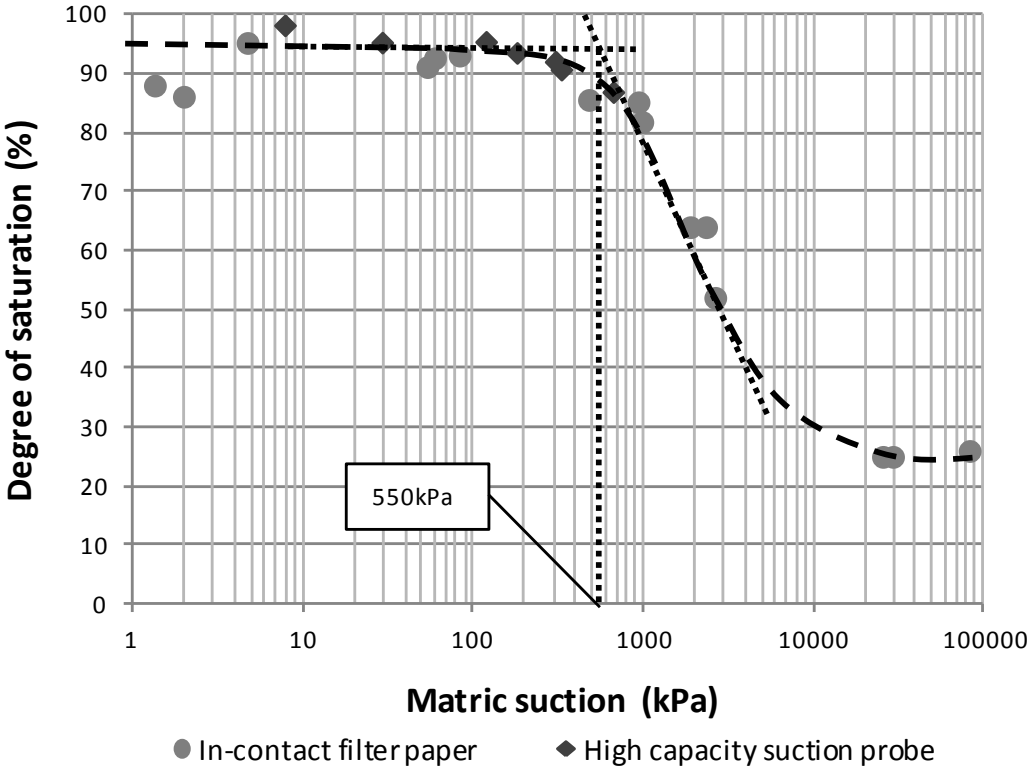

Figure 3 – Degree of saturation versus matric suction, for compacted samples staged dried from 25% of water content.

3 Sample preparation

Samples were prepared resembling construction conditions, thus the compaction curve obtained in Figure 1 was used as a reference. For normal compaction testing a mould of 115 mm high by 105mm diameter was used (BS 1377, 1990). For triaxial testing, specimens with a height:diameter ratio of 2:1 are required. To attempt a better representation of field conditions a sample size of 100mm diameter was decided on, so the sample height needed to be 200mm. The level of compaction was maintained as equivalent to the compaction testing, but a 100mm diameter by 200mm high split mould was used. Therefore, each sample was-compacted in 6 layers of approximately 33mm each (compared to 3 layers of 38mm for conventional compaction testing).

For the drying procedure, the samples were left to dry to atmosphere in temperature control conditions while the mass was continuously monitored. As soon as the target mass was reached (and hence the target water content), the sample was sealed in plastic film as to allow the water content to equalise within the sample. For the material under study, it was determined that the equalisation period to achieve a water content distribution within a ±1% tolerance was 10 days (see Mendes, 2011). The drying procedure was used to dry samples prepared at 22% of water content as-compacted to dried water contents of 20% and 15%; and samples prepared at 20% as-compacted to a dried water content of 15%.

For the wetting procedure, the samples were placed inside a humidifying chamber equipped with mini foggers inside a container filled with water. The mini foggers, when placed inside the container with water, cavitate the water through ultrasound. The generated mist, where water is in the gas phase, is slowly absorbed by the samples. Samples were left inside the humidifying chamber, but removed regularly to monitor changes in mass, until the target mass was achieved. As in the drying procedure, after the target mass was reached, the samples were then wrapped in plastic film for water content equalisation. Based on a preliminary study on water content distribution after equalisation, the equalisation period to achieve a water content distribution within the sample with a ±1% tolerance was 3 weeks (see Mendes, 2011). The wetting procedure was used to wet samples prepared at 15% of water content as-compacted to wetted water contents of 20% and 22%; and samples prepared at 20% as-compacted to wetted water contents of 22%.

4 Apparatus

4.1 Triaxial apparatus for the Consolidated Drained test series (saturated)

The consolidated drained (CD) tests on saturated samples were performed in conventional triaxial cells. Conventional triaxial cells were suited for testing since tests were performed in saturated conditions and volume changes could be measured directly from the water flow within the sample. The consolidated drainedCD triaxial tests consisted in three stages: saturation, consolidation and shearing.

Saturation was imposed by maintaining an elevated back pressure applied to the top and bottom of the sample (300kPa) while cell pressure was at a slightly higher pressure (305kPa) to maintain effective stress close to zero. The progression of saturation within the sample was determined from the evolution of the B value. To monitor the B value, the cell pressure was increased by 100kPa to 405kPa and, under undrained conditions, recording the response from the pressure transducers connected to top and bottom of the sample. When the B value reached values of 0.95, it was assumed that the sample was saturated.

In the consolidation stage, the cell pressure was increased to the desired value, while maintaining the back pressure at 300kPa. After consolidation, the sample was subjected to shearing at a constant rate of 0.005mm/min.

4.2 Triaxial apparatus for the Constant Water Content test series (unsaturated)

While the saturated tests were performed in conventional triaxial cells, the constant water content tests were performed in Wykeham Farrance double cell triaxial cells (DCTC) (Mendes et al, 2012). The two cell arrangement where the outer cell surrounds the inner cell, enables a more accurate measurement of the volume change of samples when the sample voids are not saturated. Two features makes the double cell triaxial cell a suitable piece of equipment to carry out triaxial tests on unsaturated samples: the wall of the inner cell being made in glass eliminates the water absorption problem identified in cell walls built in Perspex; and since the pressure is maintained equal in both cells (inner and outer), the pressure surrounding the wall of the inner cell will be the same, eliminating the majority of deformations of the wall cell reducing the error in the measurement of the volume changes inside the cell. In addition, the use of a high capacity suction probe in the sample pedestal enabled pore water pressure measurements to be made directly in the sample without the necessity of using elevated pore air pressures (axis translation) to simulate matric suction.

The equipment configuration for the CWC tests is schematically presented in Figure 4. Referring to Figure 4, the components used in testing were as follow:

- The confining pressure (σ_3) was imposed in the inner cell by a stepper motor driven hydraulic pump built by Wykeham Farrance. It was measured using a 2000 kPa pressure transducer C in the water pressure line; to maintain a constant pressure in the outer cell a similar configuration was adopted, resulting in both cells being completely independent from each other;
- While raising the Wykenham Farrance loading frame H at a constant rate of 0.025mm/min, rate controlled by the vertical displacement transducer E, measurements of vertical stress (σ_1) were being taken by a 10 kN capacity load cell D;
- The volumetric behaviour of the sample (ε_v) was measured at the volume gauge A. By measuring the flow of water of the inner cell the volume changes observed on the volume gauge A were caused by volumetric changes in the sample.
- Vertical deflections (ε_a) were determined from the axial displacement transducer, with 75 mm range, mounted externally. In addition, by mini linear variable differential transformers F (mini LVDT), mounted internally on the sample with a nominal range of 5mm (but actually capable of reaching 10 mm with appropriate calibration).
- Pore water pressure (u_w) was measured by a high capacity suction probe G placed at the bottom in direct contact with the sample. The high capacity suction probe was capable of direct measurement of suctions of 2MPa.
- The sample platen was a flat surface with 2 holes connected to drainage lines. The intention of these tests was to perform constant water content triaxial tests while measuring the evolution of suction using a suction probe. As the pore water pressure was measured directly by a high capacity suction probe without the implementation of axis translation there was no need to install a high air entry value stone in the platen. The drainage lines were used to allow the evacuation of air from the sample (to maintain atmospheric air pressure) during the constant water compression and shearing stages.
- The software TRIAX, a dedicated computer control system for triaxial testing (Toll, 1999), was used to control inner and outer cell pressures, loading rate of the loading frame and to record data from all the measurement equipment.

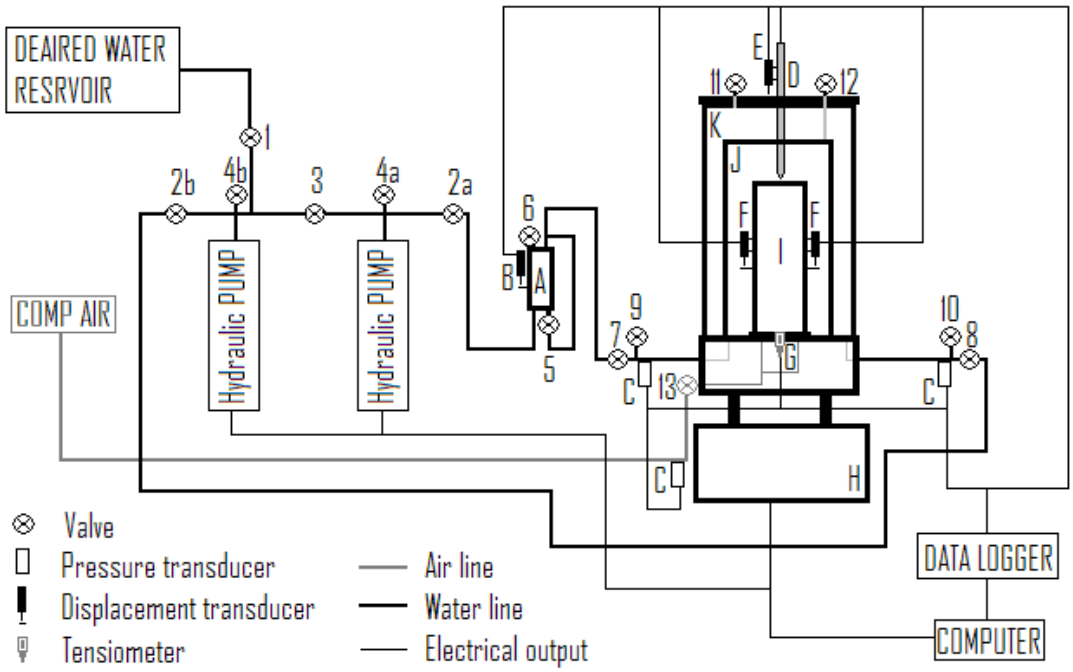

Letter	
A	Volume gauge
B	Volume change transducer
C	Pressure transducer
D	Load cell
E	Axial displacement transducer
F	Mini LVDT
G	Suction probe
H	Loading frame
I	Sample
J	Inner cell
K	Outer cell

Valves	
1	Main deaired water supply
2a	Water supply/pressure line – inner cell
2b	Water supply/pressure line – outer cell
3	Separator valve
4a	Bleeding valve – hydraulic pump
4b	Bleeding valve – hydraulic pump
5	Overlap – volume gauge
6	Bleeding valve – volume gauge
7	Main valve - inner cell
8	Main valve - outer cell
9	Drain valve - inner cell
10	Drain valve - outer cell
11	Bleeding valve – outer cell
12	Bleeding valve – inner cell
13	Compressed air supply – sample

Figure 4 – Constant water content triaxial testing apparatus.

In preliminary testing it was found that during filling of the cell a quantity of air could become trapped in the top of both inner and outer cells endangering the accuracy of the volume change measurements. Thus, before testing, the cell was pressurised to the planned confining stress (50, 150 or 300kPa) while maintaining the sample net stress close to zero (by increasing air pressure within the sample to 5 kPa below the cell pressure) so as to dissolve the trapped air into the water. The elevated air pressure was applied until the volume change readings within the cell became stable, meaning that the air inside the cell had been compressed/dissolved. After this air in the cells was dissolved, the air pressure was then reduced back to zero while maintaining the same cell pressure, in the process applying the required stress conditions for the constant water content compression stage. Further details of the Wykenham Farrance double cell triaxial cells can be found in Mendes et al. (2012).

When the equilibrium within the cell due to the presence of air was achieved, the constant water content tests started. The constant water content tests were performed in two stages: constant water content compression followed by shearing. The constant water content compression stage was performed under isotropic conditions at fixed confining pressures (50, 150 and 300kPa). Each sample was compressed until the sample volume change rate was equal or lower than 0.004cm^3/hr for a 24hr period, a change rate equal to the creep in the triaxial cell observed by Mendes et al (2012). In the shearing stage, the shearing rate used in the CWC tests was 0.025mm/min.

5 Consolidated drained triaxial test series (saturated)

Conventional consolidated drained (CD) tests were performed on fully saturated samples. 38mm diameter by 76mm high samples were used for this saturated series of tests. The samples were initially prepared according to the sample preparation methodology presented earlier and then subsequently cored from larger samples (100mm diameter by 200mm high). The consolidated drained tests were carried out on samples that were prepared at as-compacted water contents of 15%, 20% and 22% and later saturated inside the triaxial apparatus. The tests were repeated for three different confining pressures: 50kPa, 150kPa and 300kPa.

The CD triaxial testing program is presented in Table 1. The initial conditions of each sample prior to testing are also presented in Table 1.

Table 1 – Triaxial testing program for the CD test series, showing testing conditions.

Test no.*	As-compacted					
	Water Content	Density		Void ratio	Degree of Saturation	Confining pressure
		Bulk	Dry			
	$w_{(ac)}$	ρ	ρ_d	e	Sr	
	%	Mg/m^3	Mg/m^3	-	%	kPa
S15(50)	14.63	2.164	1.888	0.43	92	50
S15(150)	14.75	2.176	1.896	0.43	94	150
S15(300)	14.75	2.142	1.867	0.45	89	300
S20(50)	19.70	2.029	1.695	0.59	90	50
S20(150)	19.70	2.032	1.697	0.59	90	150
S20(300)	19.70	2.020	1.687	0.60	88	300
S22(50)	21.78	2.052	1.685	0.60	97	50
S22(150)	21.78	2.032	1.669	0.62	95	150
S22(300)	21.78	2.041	1.676	0.61	96	300

* Each test is identified in the form of Sxx(yy) by the as-compacted water content (xx) and confining pressure applied during the test (yy).

Figures 5, 6 and 7 present the test results for the shearing stage of the CD testing series. Figure 5 shows the deviator stress-axial strain (q- ε_a) curves. It can be observed that the tests S15 (at the lowest compaction water content of 15%) show the stiffest behaviour with peak strength occurred at lower axial strains (from 3% at 50kPa up to 8% at 300kPa of confining stress) than for the tests S20 and S22. For the samples compacted wet of optimum, i.e. S20 and S22 tests, the values of axial strain at failure were between 10% at 50kPa up to 17% at 300kPa of confinement.

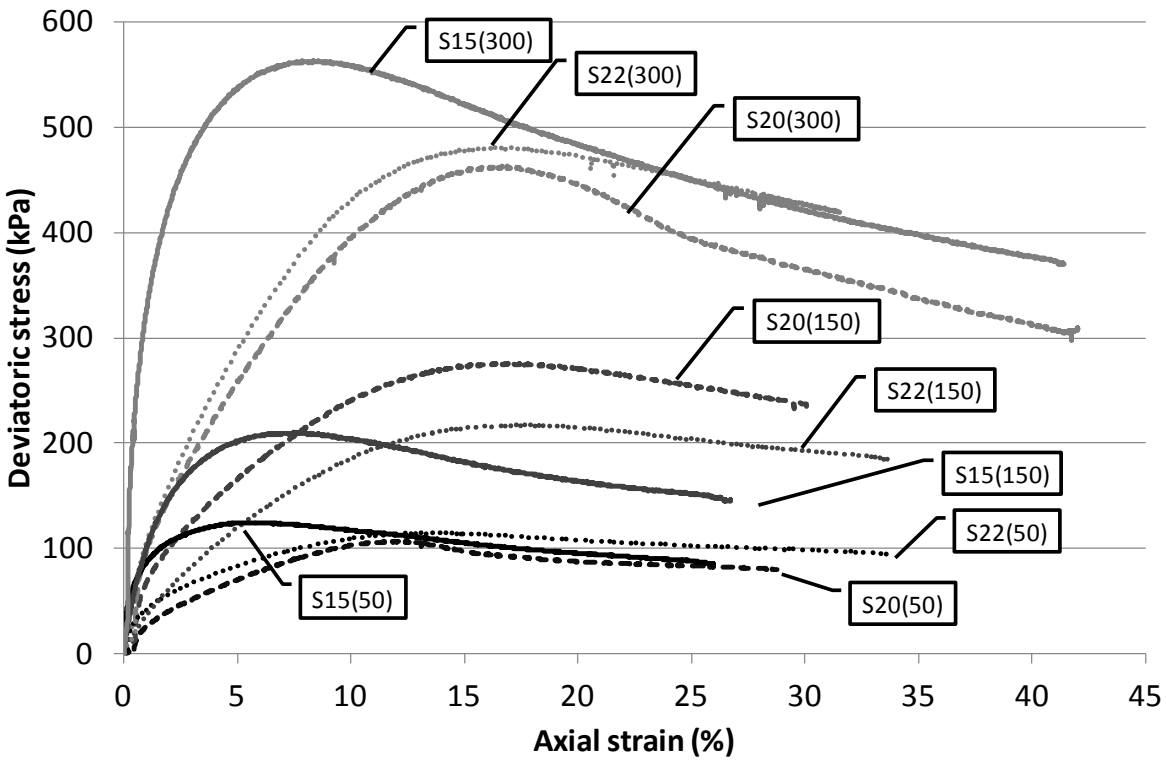

Figure 5 - Deviatoric stress-strain relationships for the CD test series.

Figure 6 presents the relation between axial and volumetric strains developed through the shearing stage of each test (compressive strains are shown as positive). At the end of the shearing stage it can be observed that, for the majority of the samples tested, volume was still changing, especially for the samples (S15) prepared at 15% of water content. More dilatant behaviour was observed in the S15 specimens.

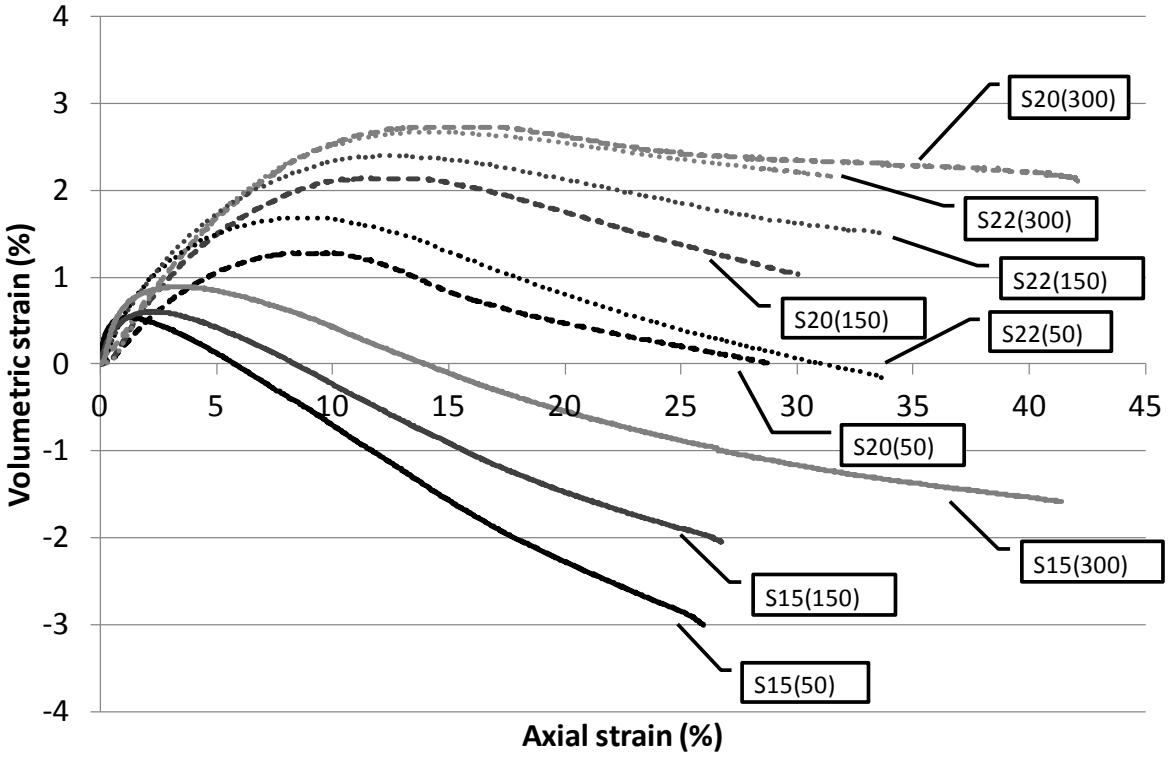

Figure 6 - Volumetric-axial strain relationships for CD test series.

The stress paths for the S15, S20 and S22 tests are shown respectively in Figures 7a, 7b and 7c. The end points of each test, taken to be the Critical State points, are shown by symbols on the plots and a best fit Critical State line is shown for each compaction water content. The critical state points were achieved at high values of axial strain (ε_a), from 25% up to 40%. At such large axial strains there can be concerns about non-uniformity of deformations and constraints due to boundary conditions. However, strains in excess of 25% are needed before the deviator stress and volumetric strains start to level off at constant values suggesting the Critical State is being achieved.

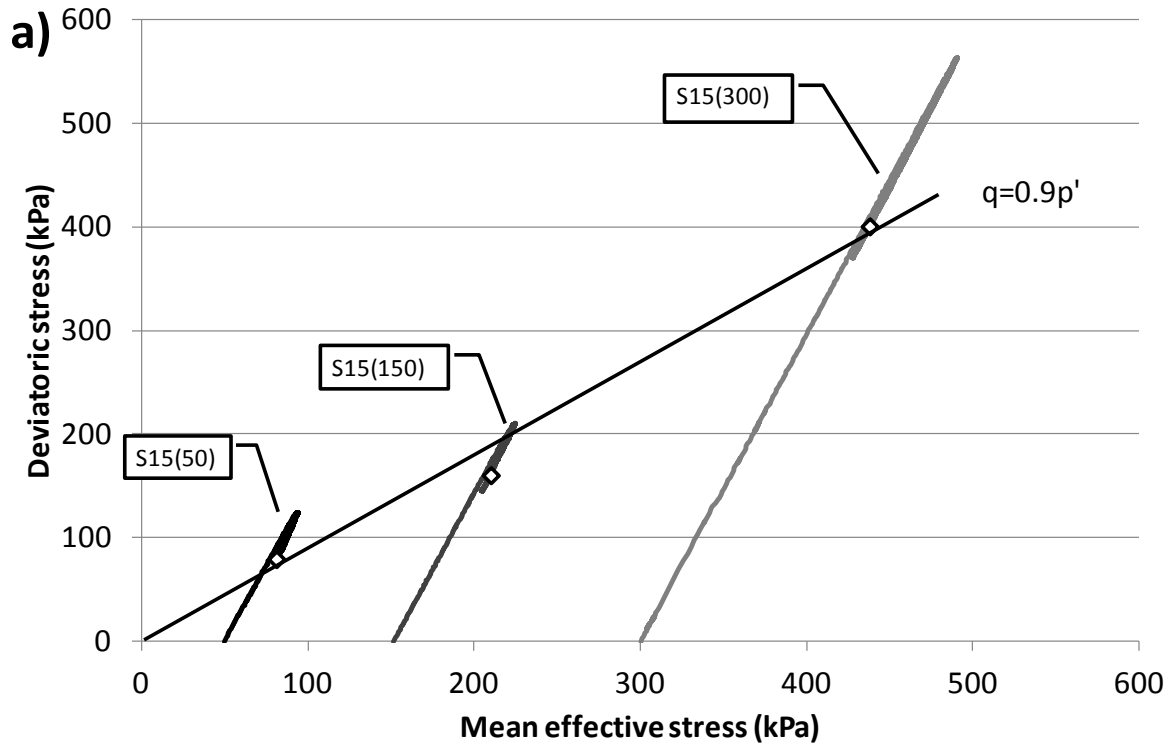

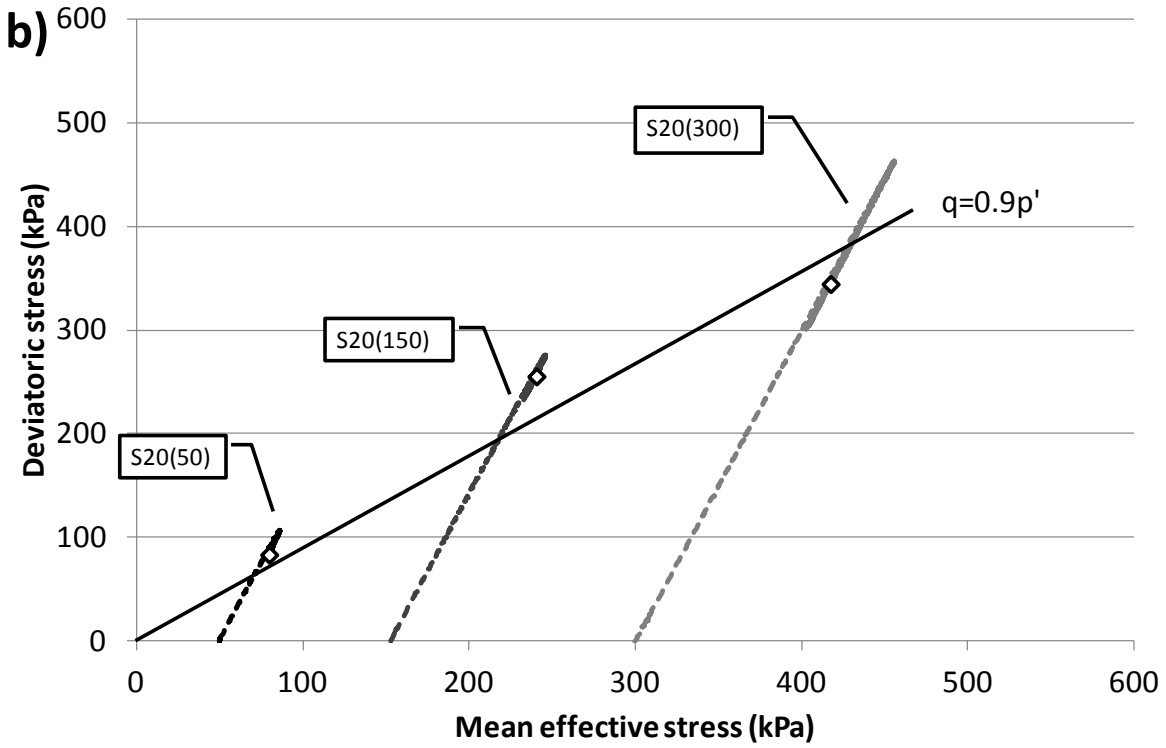

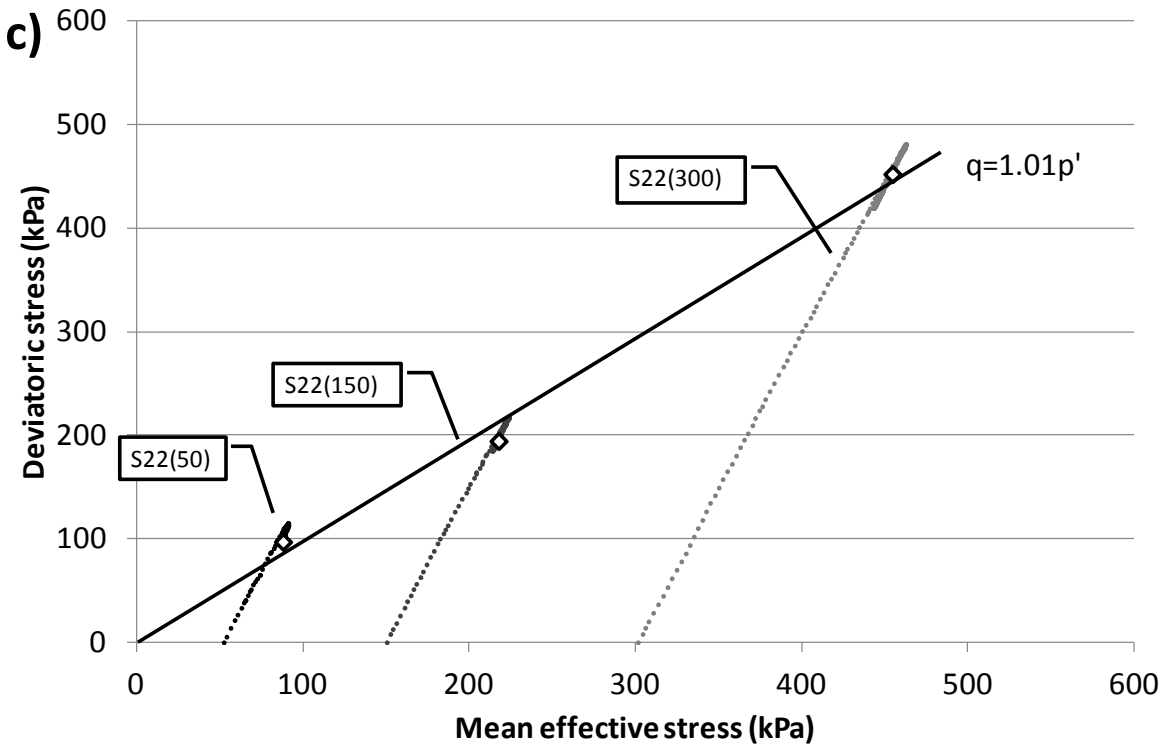

Figure 7 – Stress paths for the CD test series: **a)** as-compacted water content of 15%; **b)** as-compacted water content of 20%; **c)** as-compacted water content of 22%.

It can also be seen in Figures 7 (a-c) that the slope of the CSL in the plane q – p', M, was found to be 0.90 for samples saturated from water contents of 15% and 20% and 1.01 for samples saturated from 22%. An average value of M=0.93 was taken to represent saturated conditions.

The final specific volume (ν) values from each test are plotted against mean effective stress, p' in Figure 8. The slope of the critical state lines (CSL) in the ν – p' plane (λ) was found to be 0.05 for samples saturated from 22%, 0.06 for the samples saturated from 15% and 0.07 for samples saturated from 20% with intercepts (Γ) of 1.82 for samples saturated from 22% and 1.87 for samples saturated from 15% and 20%.

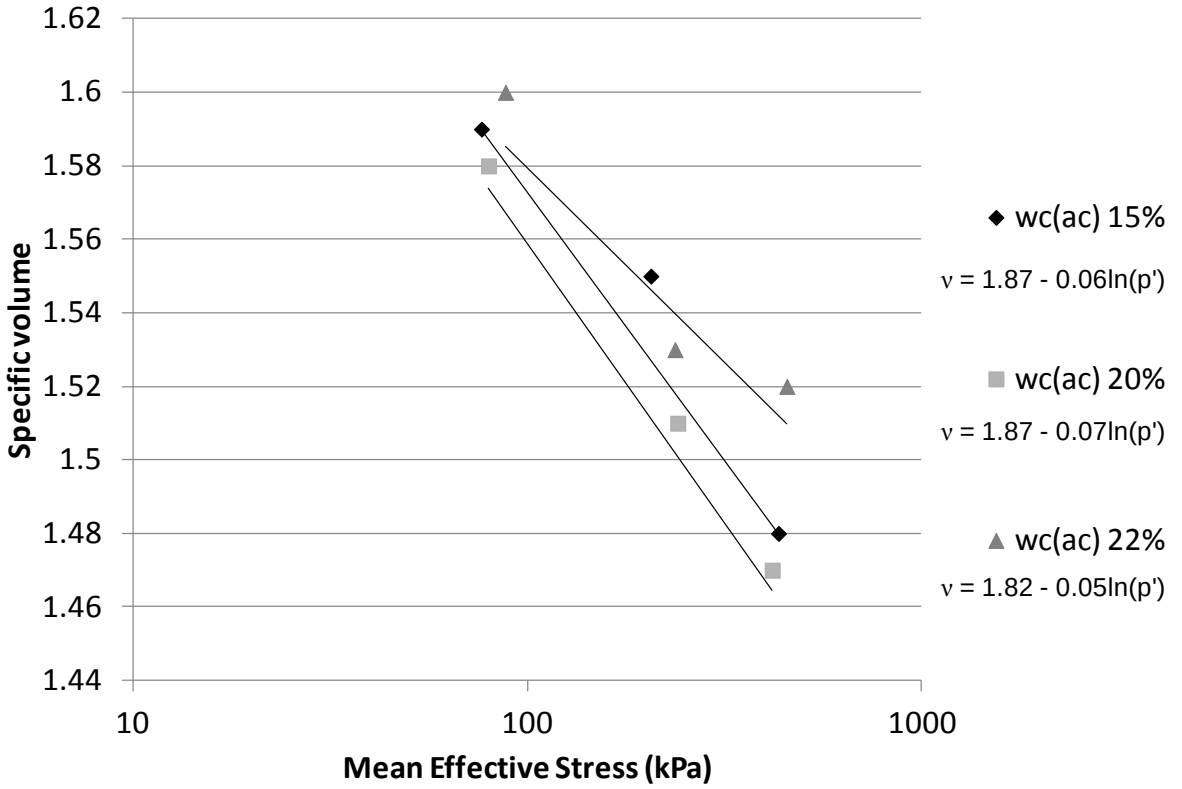

Figure 8 – Critical state line of the CD test series in ν- p' plane.

Best fit values for the intercept of the critical state line in ν axis (Γ) and slope of the critical state lines in the ν – p' plane (λ) of Γ =1.87 and λ=0.06 were taken to represent saturated conditions.

It has to be recognised that identifying Critical State conditions in dense compacted soils will always be difficult. Even at large strains (>25%) there are still changes in deviator stress and volume strain. At the higher stress level (300kPa) particularly, the deviator stress is still falling at the end of the test (Figure 5). However, for these tests the volume strain response does tend to level off at around 30% strain (Figure 6). It is likely that the point of levelling off of volume strain could represent the Critical State, with the continuing fall in deviator stress being caused by strain localisation due to the formation of shear surfaces (i.e. moving from Critical State towards a Residual State). By considering all the test data, it is felt that the average parameters of M=0.93, Γ =1.87 and λ=0.06 give the best representation of the Critical State for saturated samples.

6 Constant water content test series (unsaturated)

The CWC triaxial tests samples were tested as-compacted at the water contents of 15%, 20% and 22%. Further samples were tested where water content was changed either by wetting or drying after compaction. These tests included: samples wetted to 20% and 22% from 15% as-compacted

water content; samples dried to 15% and wetted to 22% from 20% as-compacted water content; and, samples dried to 15% and 20% from 22% as-compacted water content. The CWC triaxial tests were repeated for three different confining pressures: 50kPa, 150kPa and 300kPa.

As for the CD testing series each test was indentified in the forms Cxx(yy) by the as-compacted water content (xx) and confining pressure (yy) for samples tested as-compacted, Dxx(yy) for samples dried from as-compacted conditions and Wxx(yy) for samples wetted from as-compacted conditions. Where two replicate tests were performed at the same water content and confining stress, these are indicated by an additional test number, such as C15(50) 1 and C15(50) 2.

Tables 2, 3 and 4 present the initial conditions of the samples at the start of each CWC test. These initial conditions refer to the point when the samples were placed inside the triaxial cell, where $w_{(ac)}$ and w_i represent water content obtained after compaction and initial water content at the start of the test. The initial suction is also presented.

Table 2 –Initial conditions at the start of the constant water tests for samples compacted at 15%.

Test No.	Water Content		Dry density	Void ratio	Degree of Saturation	Initial Suction
	w_{ac} %	w_i %	ρ_d Mg/m^3	e	S_r %	s_i kPa
C15(50) 1	14.77	14.77	1.839	0.47	87.91	227
C15(50) 2	14.75	14.75	1.831	0.48	83.77	420
C15(150)	15.17	15.17	1.815	0.49	83.80	255
C15(300)	14.62	14.62	1.837	0.47	83.87	420
W15-19(150)	15.21	18.45	1.715	0.58	93.83	7
W15-19(300)	15.44	19.37	1.693	0.60	90.56	17
W15-20(50)	14.61	19.70	1.732	0.56	96.51	35
W15-20(150)	15.09	19.75	1.667	0.62	95.84	3
W15-22(50)	14.67	22.00	1.659	0.63	94.43	0.3

Table 3 –Initial conditions at the start of the constant water tests for samples compacted at 20%.

Test No.	Water content		Dry density	Void ratio	Degree of Saturation	Initial Suction
	w_{ac} %	w_i %	ρ_d Mg/m^3	e	S_r %	s_i kPa
C20(300)	20.17	20.17	1.709	0.58	93.69	18
D20-15(150)	19.15	15.56	1.792	0.51	82.76	264
D20-15(300)	18.75	15.19	1.816	0.49	84.05	350
W20-21(150)	19.24	20.68	1.677	0.61	95.12	4
W20-22(50)	19.40	21.53	1.709	0.58	96.08	4
W20-22(300)	19.89	21.29	1.670	0.62	92.99	5

Table 4 –Initial conditions at the start of the constant water tests for samples compacted at 22%.

Test No.	Water content		Dry density	Void ratio	Degree of Saturation	Initial Suction
	w_{ac} %	w_i %	ρ_d Mg/m^3	e	S_r %	s_i kPa
C22(50)	21.82	21.82	1.621	0.67	88.34	5
C22(150)	22.16	22.16	1.609	0.68	88.03	7
C22(300)	22.01	22.01	1.624	0.66	89.50	7
D22-20(150) 1	21.92	19.78	1.680	0.61	87.80	2.5
D22-20(150) 2	22.09	20.08	1.649	0.64	84.94	107
D22-19(150)	21.37	19.04	1.651	0.64	80.84	91
D22-16(50)	21.45	16.84	1.782	0.52	88.13	
D22-16(300)	21.00	15.80	1.811	0.49	86.65	131
D22-14 (150)	21.74	13.97	1.830	0.48	79.18	243

Figures 9, 14 and 19 show the stress-strain relationships for the constant water content tests. The shearing stage in each test started with a rapid increase of deviatoric stress over a small range of the axial strain which was followed by a continued increase in deviatoric stress at higher axial strains. After these two phases of increase of deviatoric stress two different end conditions were observed: the first was observed in the samples that had w_i close to 15% (C15(50) 1, C15(50) 2, C15(150), and C15(300) in Figure 9; D20-15(150) and D20-15(300) in Figure 14 and D22-16(50), D22-16(300) and D22-14(150) in Figure 19) where a distinct peak in deviator stress was followed by an abrupt decline of the deviatoric stress over a short range of axial strain followed by a continued reduction in deviatoric stress at higher axial strains; for the remaining tests after the maximum deviatoric stress was achieved, the deviatoric stress was maintained at almost a constant level, with no sign of strain softening.

In general the tendency for pore water pressure behaviour during the shearing stages was similar in all tests. Pore water pressure increased with an initial contraction in volume as the load was initially applied and, when samples started to dilate, it produced a decrease in pore water pressure, see Figures 10 and 11, for tests performed on samples with w_{ac} close to 15%; Figures 15 and 16, for tests performed on samples with w_{ac} close to 20%; Figures 20 and 21, for tests performed on samples with w_{ac} 22%.

The stress path achieved in each test is presented in Figure 12 (for samples prepared from samples with $w_{(ac)}$ close to 15%), Figure 17 (for samples prepared from samples with $w_{(ac)}$ close to 20%) and Figure 22 (for samples prepared from samples with $w_{(ac)}$ close to 22%) where, $p\text{-}u_w$ represents mean net stress minus pore water pressure. In the case of saturated tests it would be mean effective stress, however, as the specimens were not saturated, $p\text{-}u_w$ cannot be taken as effective stress. As expected, samples that were tested at w_i close to 15%, had the higher values of suction in this testing program (lowest values of pore water pressure) experienced the largest changes in deviatoric stress. In contrast, samples with w_i close to 22% experienced the lowest changes of deviatoric stress and $p\text{-}u_w$.

Changes in void ratio experienced during shearing by each test are presented in Figures 13, 18 and 23.

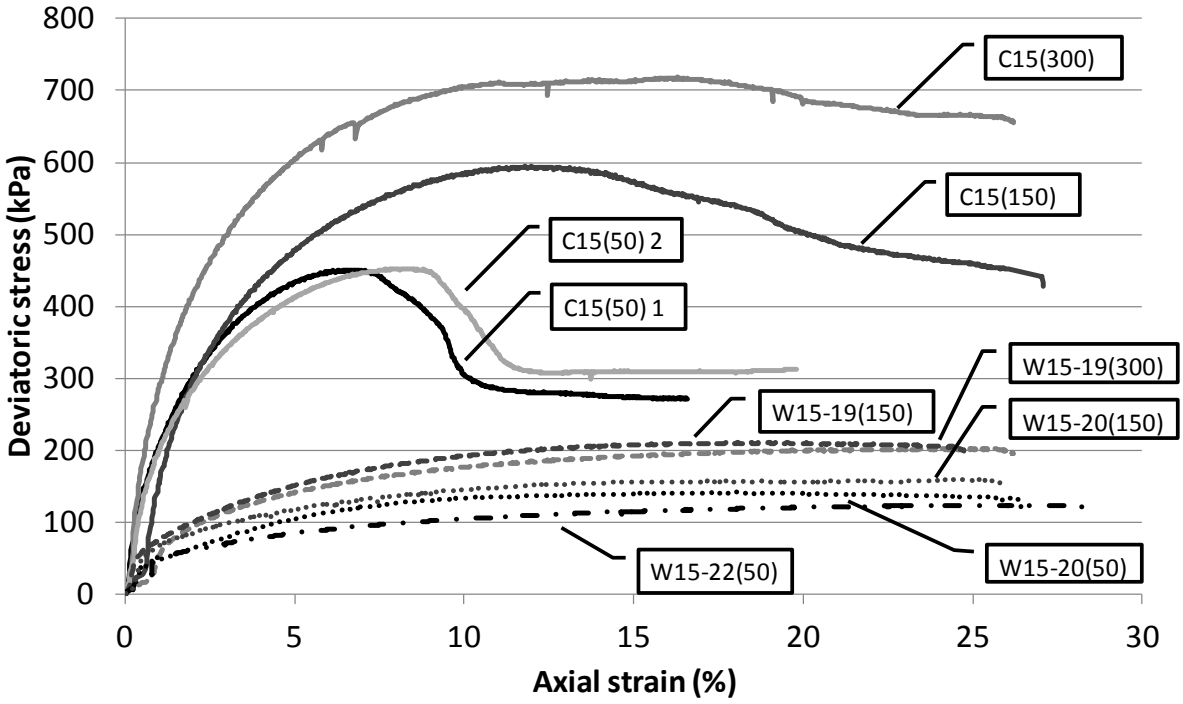

Figure 9 – Deviatoric stress- strain relationships for samples with $w_{(ac)}$ of 15%.

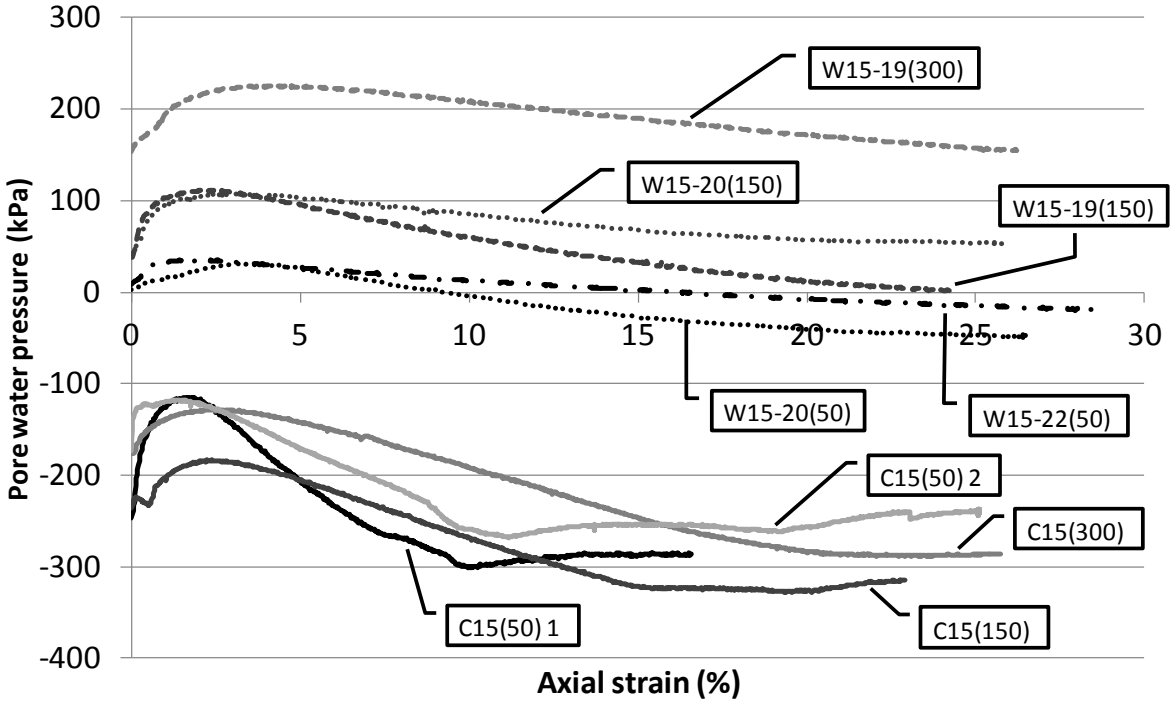

Figure 10 – Variation of pore water pressure with axial strain for samples with $w_{(ac)}$ of 15%.

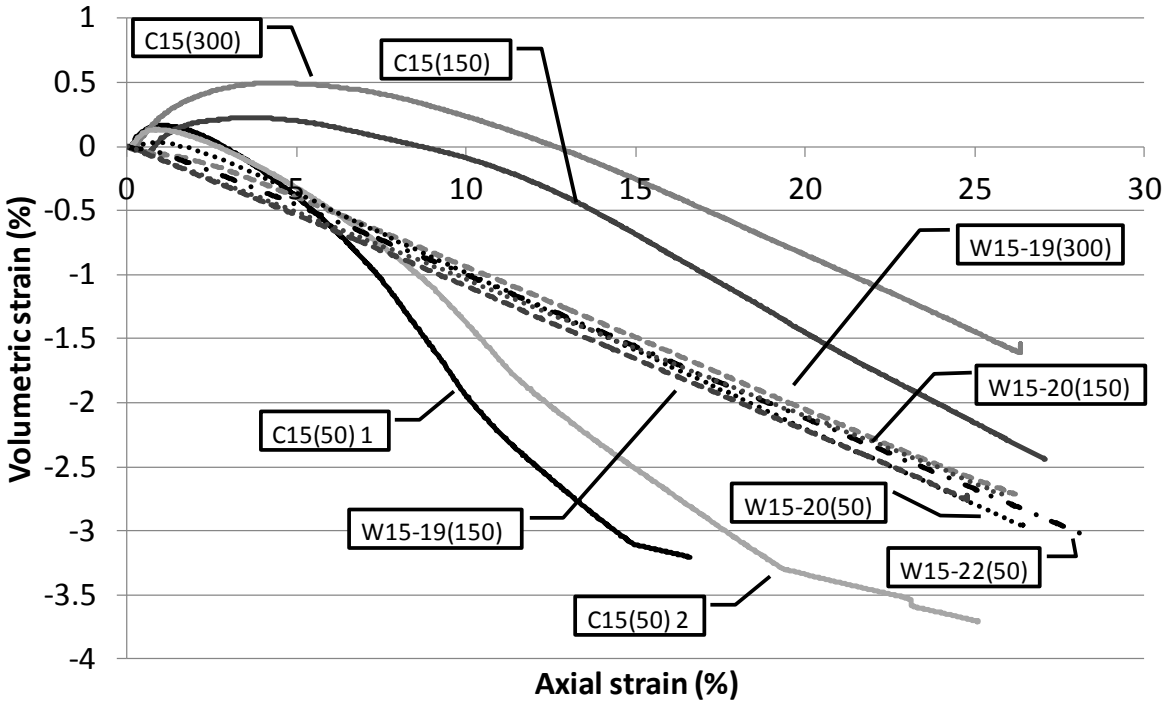

Figure 11 – Volumetric-axial strain relationships for samples with $w_{(ac)}$ of 15%.

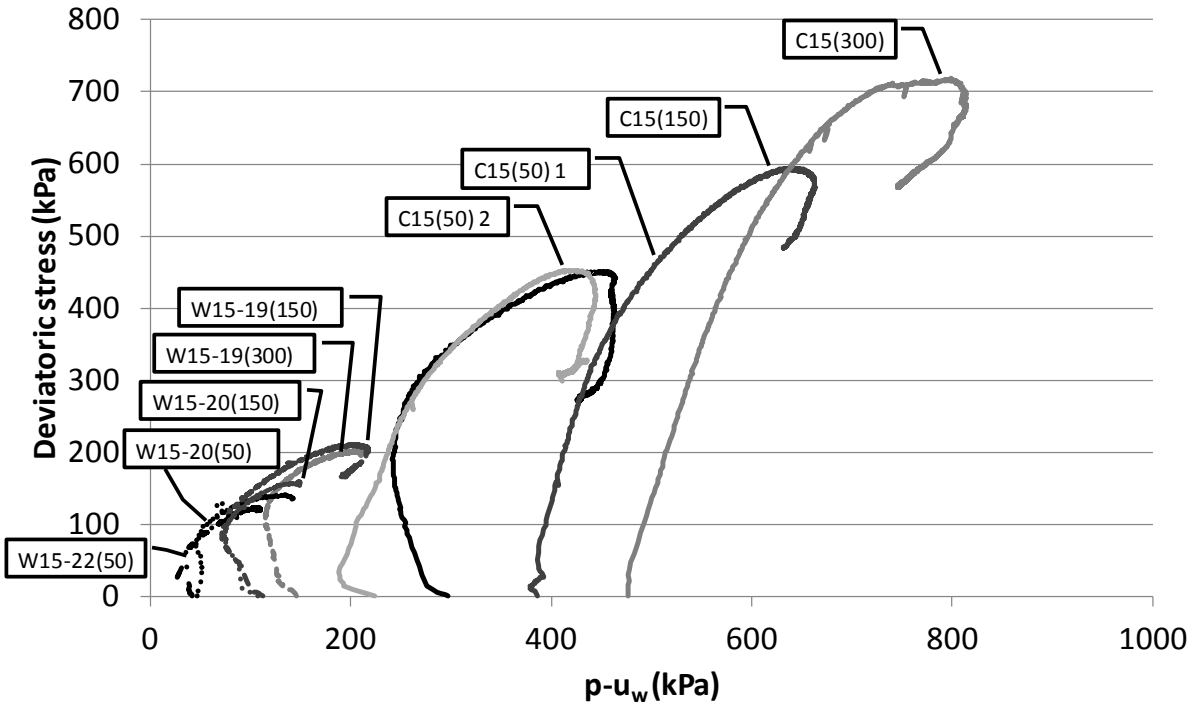

Figure 12 – Constant water content stress paths in the ($p-u_w$)-q plane for samples with $w_{(ac)}$ close to 15%.

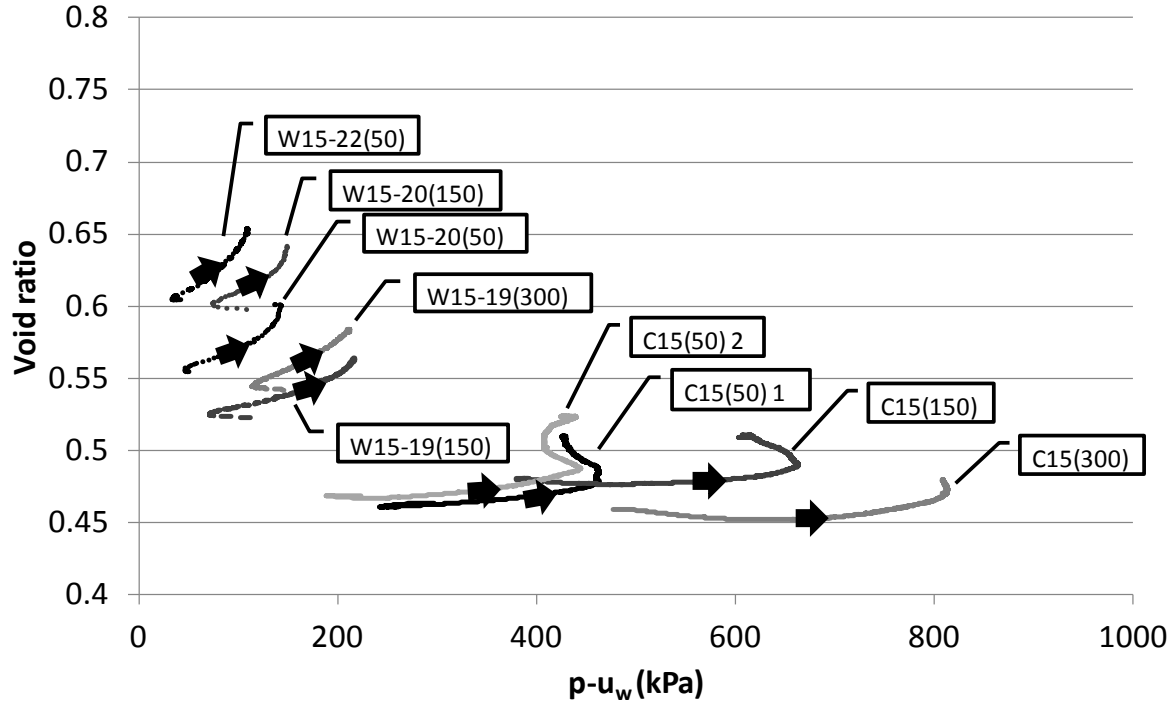

Figure 13 – Void ratio - ($p-u_w$) relationships for samples with $w_{(ac)}$ of 15%.

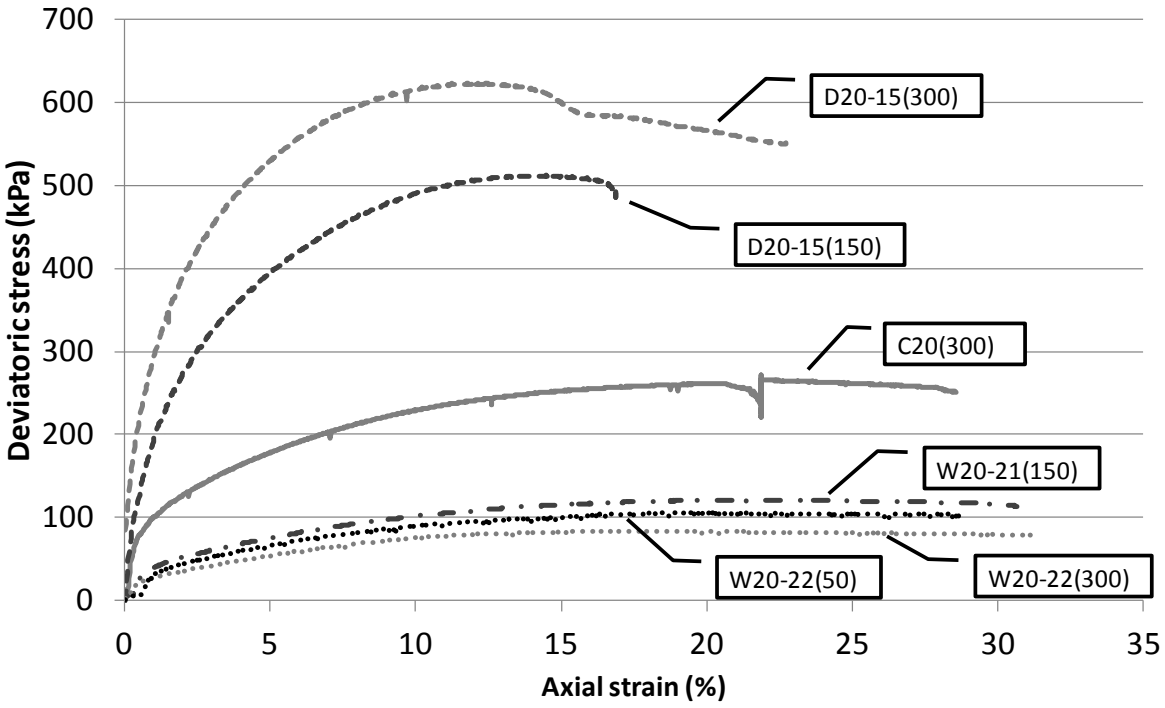

Figure 14 – Deviatoric stress- strain relationships for samples with $w_{(ac)}$ of 20%.

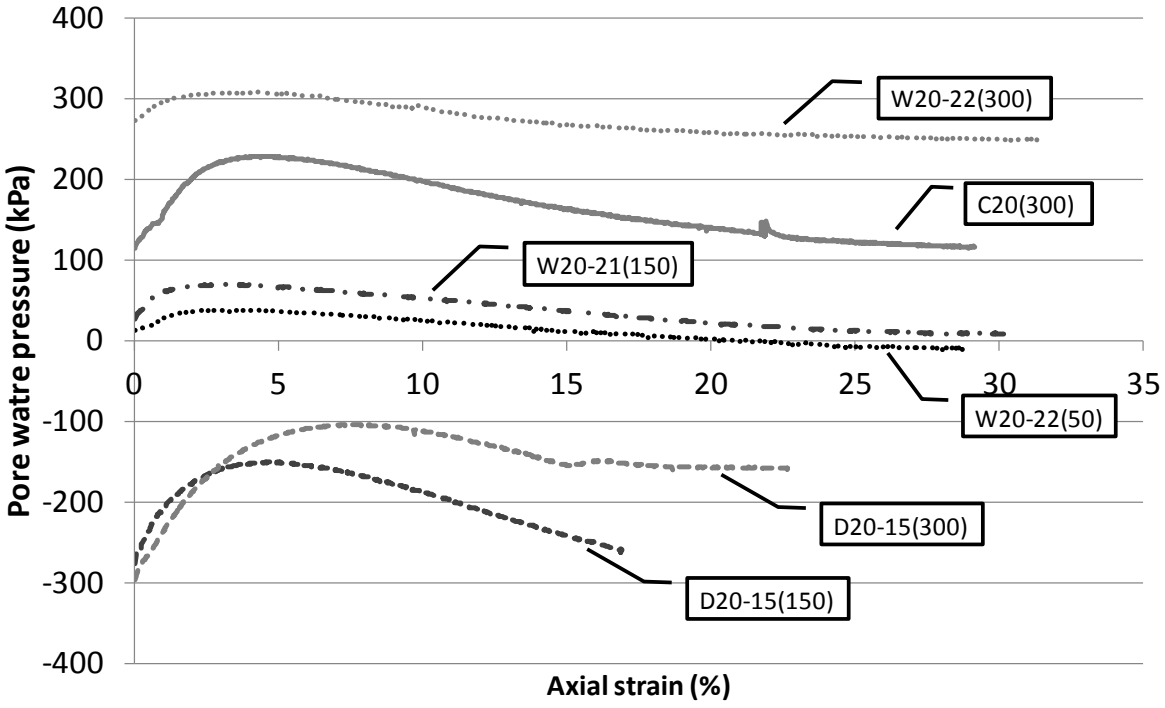

Figure 15 – Variation of pore water pressure with axial strain for samples with $w_{(ac)}$ of 20%.

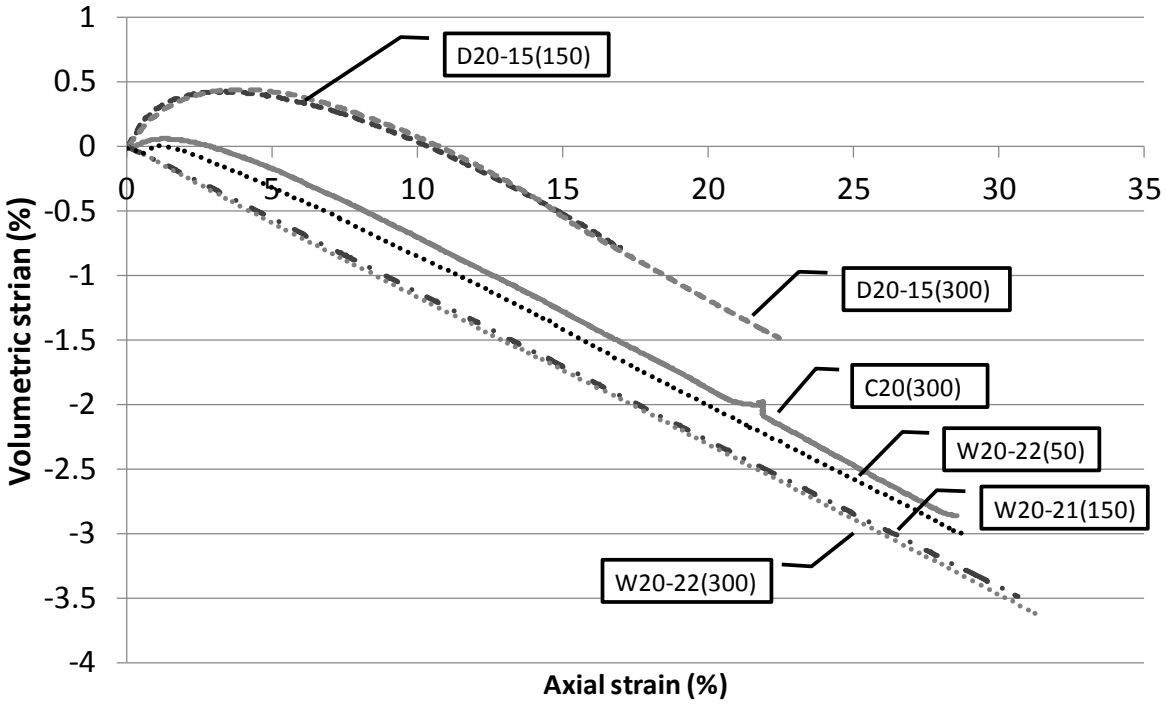

Figure 16 – Volumetric-axial strain relationships for samples with $w_{(ac)}$ of 20%.

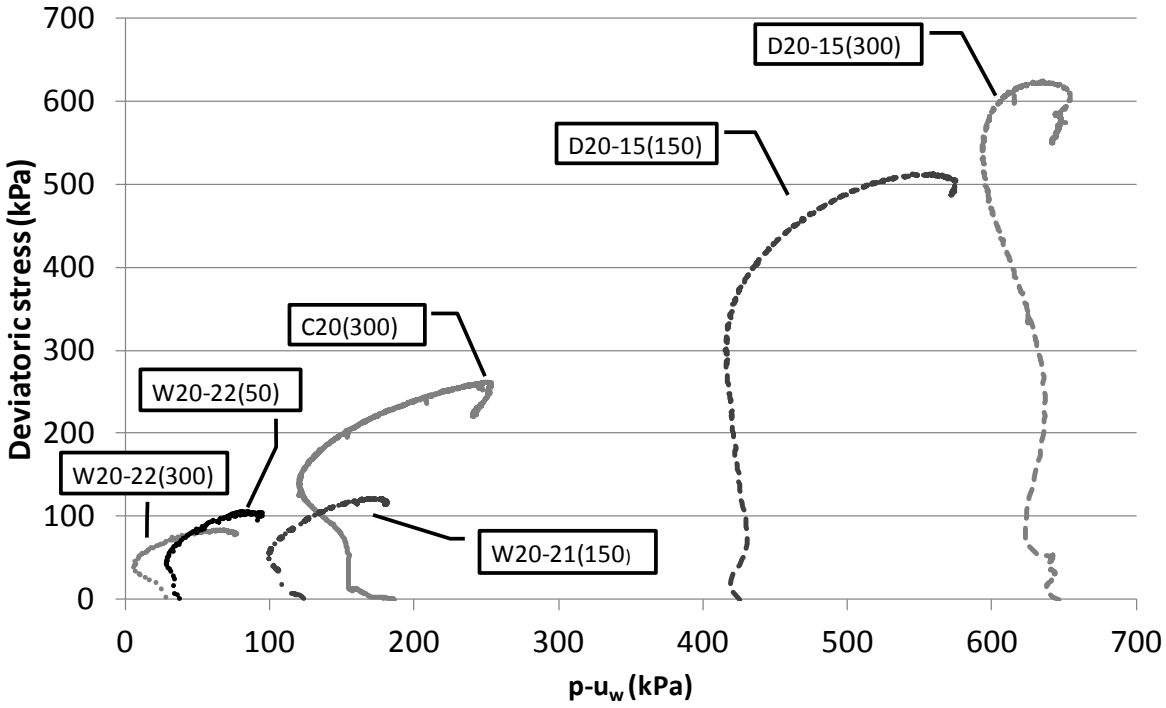

Figure 17 – Constant water content stress paths in the ($p-u_w$)-q plane for samples with $w_{(ac)}$ close to 20%.

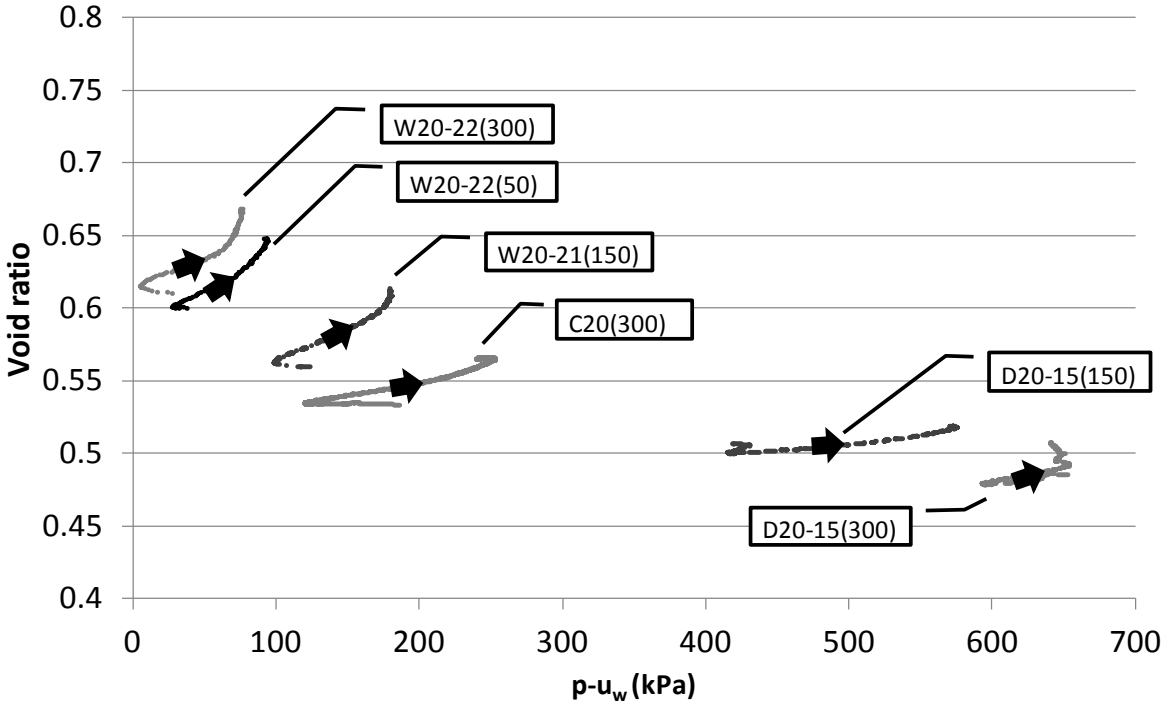

Figure 18 – Void ratio - ($p-u_w$) relationships for samples with $w_{(ac)}$ of 20%.

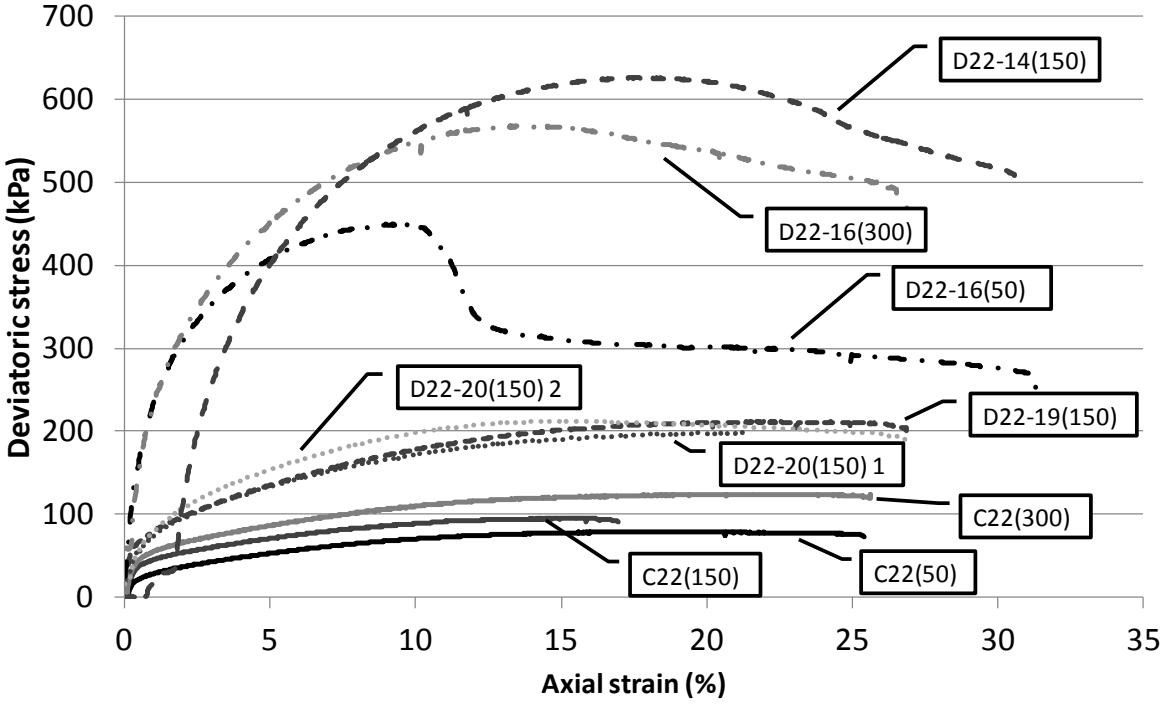

Figure 19 – Deviatoric stress- strain relationships for samples with $w_{(ac)}$ of 22%.

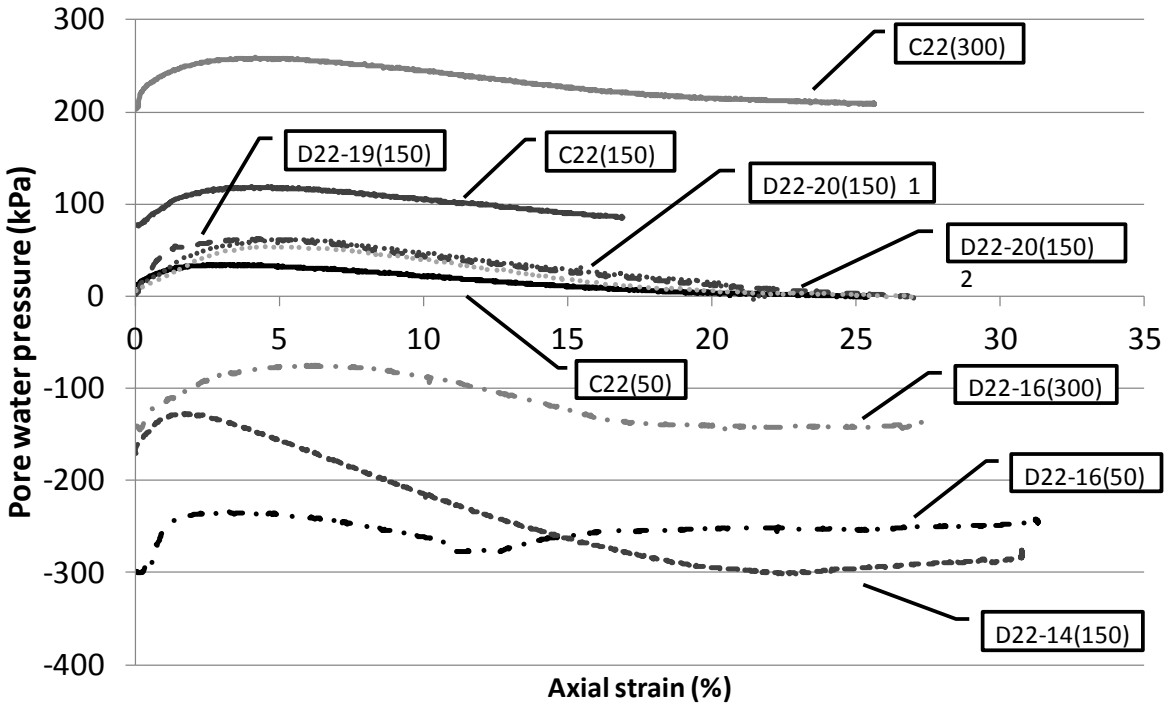

Figure 20 – Variation of pore water pressure with axial strain for samples with $w_{(ac)}$ of 22%.

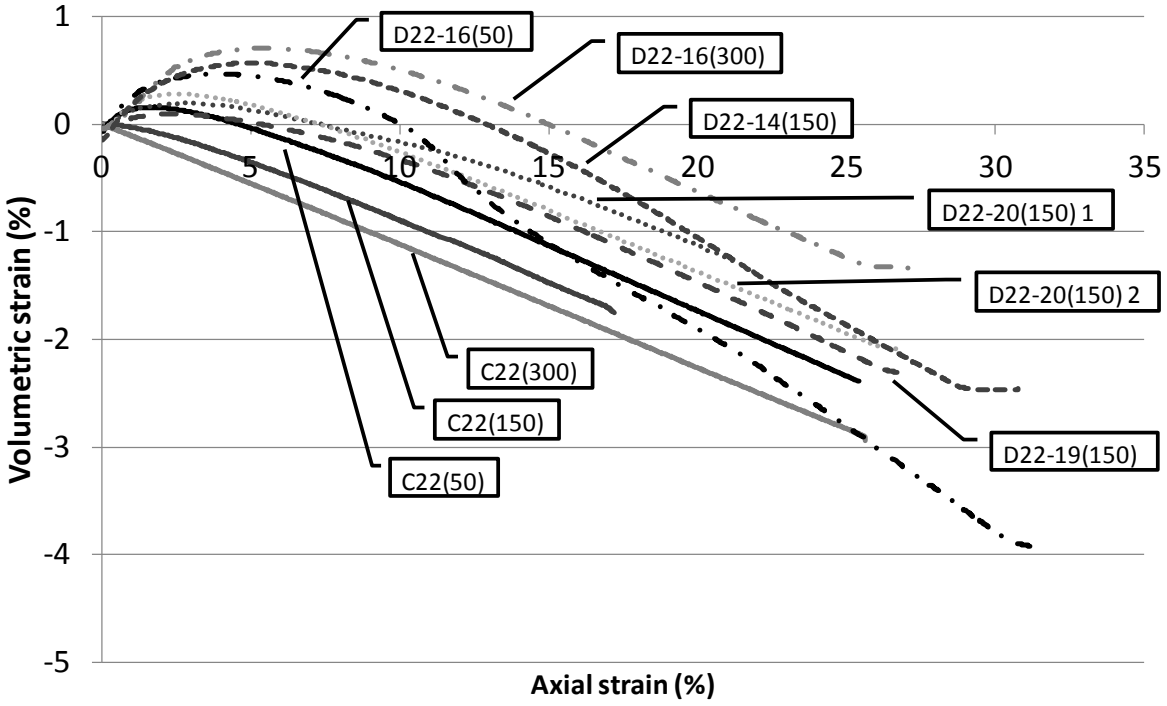

Figure 21 – Volumetric-axial strain relationships for samples with $w_{(ac)}$ of 22%.

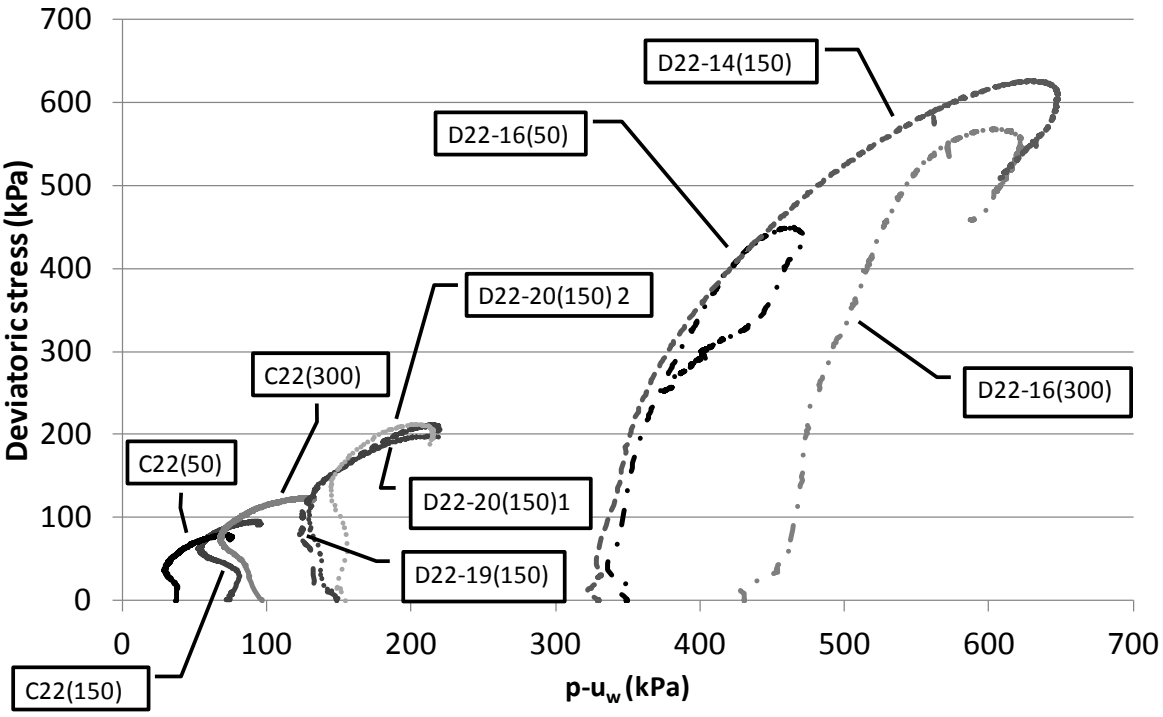

Figure 22 – Constant water content stress paths in the (p-u_w)-q plane for samples with $w_{(ac)}$ close to 22%.

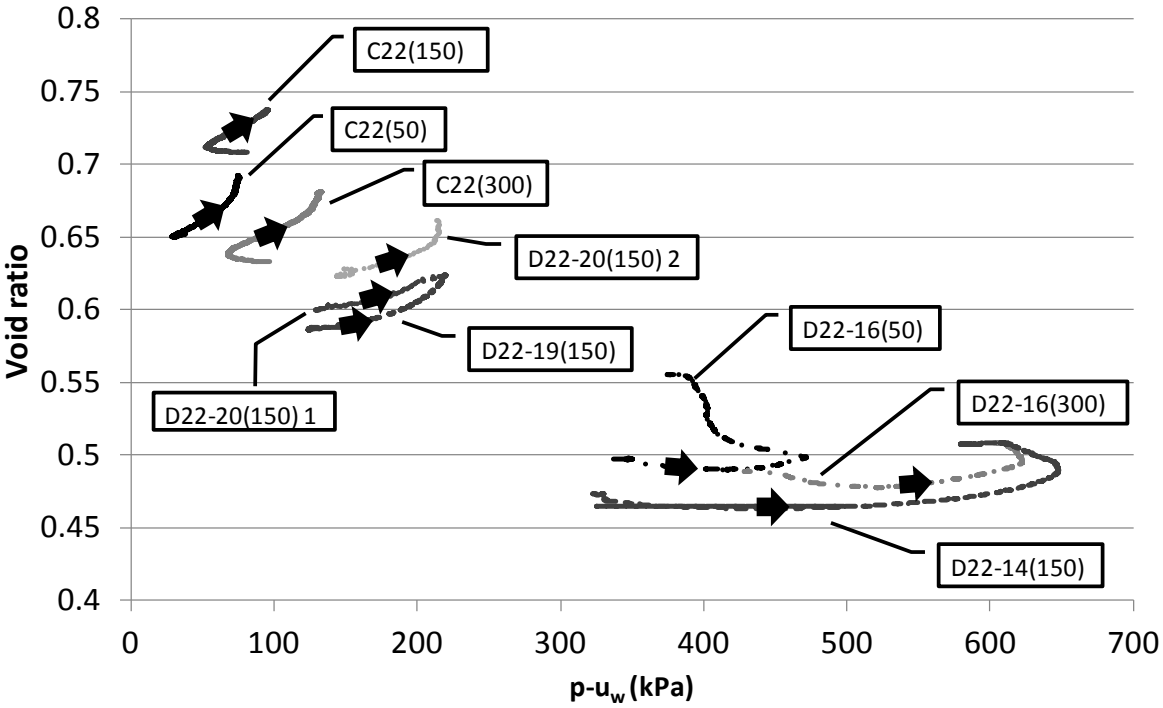

Figure 23 – Void ratio - (p-u_w) relationships for samples with $w_{(ac)}$ of 22%.

The peaks in stress-strain behaviour observed during shearing, see Figures 9, 14 and 19, on samples tested at a w_i close to 15%, were shown by samples with values of pore water pressure that were negative at the start of shearing, from: samples tested as-compacted at 15% of water content (tests C15(50) 1, C15(50) 2, C15(150) and C15(300) in Figure 9); and samples compacted at water contents

of 20% and 22% and dried to 15% (tests D20-15(150) and D20-15(300) in Figure 14 and tests D22-16(50), D22-16(300) and D22-14(150) in Figure 19). The drying resulted in much larger pore water pressure reduction reaching negative pore water pressures large enough to be maintained during shearing.

Strength peaks were not evident in the remaining tests i.e. in tests where the w_i was 20% or 22%, in which pore water pressure was mainly positive from the start. During the shearing stage, as is observable in Figures 10, 15 and 20, even samples that had small negative values of pore water pressure after the compression stage increased to positive values during shearing.

The patterns of deviatoric stress with axial strain in Figures 9, 14 and 19 can be explained by the modes of failure. The samples tested at a w_i close to 15%, as Figure 24 illustrates, failed by the formation of a shear surface, resulting in the strength peaks and brittleness that can be seen in the stress strain relationships. Other samples that failed by bulging symmetrically under considerable deformations in a plastic and ductile manner and reached higher values of axial strain without the formation of shear planes, see Figure 25.

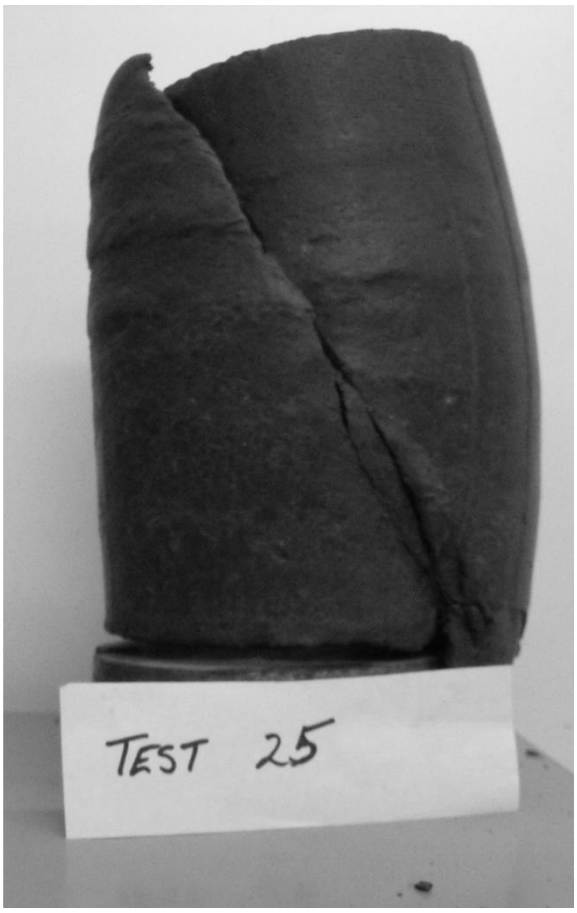

Figure 24 – Typical shape of failure on samples tested for with w_i close to 15%.

Figure 25 – Typical shape of failure on samples tested with w_i close to 20% and 22%.

7 Critical State Line

The conditions of the samples at the Critical State are shown in Table 5, 6 and 7. The type of failure, under unsaturated conditions observed in the CWC tests, implied different approaches. For the CWC tests in which samples bulged, samples failed in a ductile manner. The systematic deformations mean that the variables based on principal stresses and strains were appropriate in describing the

mechanical behaviour, as stresses and deformations can be assumed to be reasonably uniform throughout the specimen. For the CWC tests in which samples developed shear surfaces, there would be concerns that the deformations become highly non-uniform, and the overall stresses and strains no-longer represent the specimen as a whole. In this case, the assessment of the critical state point was based on an analysis of each test, mainly on Figures 13, 18 and 23 for the constant water content tests C15(50) 1, C(50) 2, C15(150), C15(300), D20-15(150), D20-15(300), D22-16(50), D22-16(300) and D22-14(150) to determine the point whenever the void ratio changed dramatically. It was assumed that behaviour after this point could no longer represent the Critical State.

Table 5 – Critical State parameters for samples with $w_{(ac)}$ close to 15%.

Test No.	$w_{(ac)}$ %	w_i %	p kPa	u_w kPa	$p-u_w$ kPa	p^* kPa	q kPa	e	v 1+e	Sr (%)
C15(50) 1	14.77	14.77	169.3	-291.7	461.0	407.8	357.5	0.49	1.49	81.76
C15(50)2	14.75	14.75	190.7	-252.8	443.5	397.7	421.7	0.49	1.49	81.89
C15(150)	15.17	15.17	324.0	-326.7	650.7	592.5	521.7	0.50	1.50	82.19
C15(300)	14.62	14.62	521.3	-286.1	807.4	756.2	663.7	0.48	1.48	82.12
W15-19(150)	15.21	18.45	217.4	0.3	217.1	217.1	202.0	0.56	1.56	88.37
W15-19(300)	15.44	19.37	365.5	156.1	209.4	225.5	196.6	0.58	1.58	89.69
W15-20(50)	14.61	19.70	90.3	-48.0	138.3	133.2	120.8	0.60	1.60	89.39
W15-20(150)	15.09	19.75	201.5	52.8	148.7	157.5	154.7	0.64	1.64	83.24
W15-22(50)	14.67	22.00	89.5	-19.5	109.0	107.3	118.7	0.65	1.65	91.03

Table 6 – Critical State parameters for samples with $w_{(ac)}$ close to 20%.

Test No.	$w_{(ac)}$ %	w_i %	p kPa	u_w kPa	$p-u_w$ kPa	p^* kPa	q kPa	e	v 1+e	Sr (%)
C20(300)	20.17	20.17	384.1	117.3	266.7	273.5	251.8	0.58	1.58	94.25
D20-15(150)	19.15	15.56	312.5	-259.3	571.8	527.0	487.3	0.51	1.51	82.73
D20-15(300)	18.75	15.19	487.4	-157.1	644.6	618.1	562.3	0.49	1.49	83.19
W20-22(50)	19.4	21.53	85.3	-9.6	94.9	93.8	91.2	0.66	1.66	88.44
W20-22(300)	19.89	21.29	328.8	250.3	78.5	117.9	76.0	0.68	1.68	84.25
W20-21(150)	19.24	20.68	188.4	8.5	179.9	180.7	115.1	0.61	1.61	91.13

Table 7 – Critical State parameters for samples with $w_{(ac)}$ close to 22%.

Test No.	$w_{(ac)}$ %	w_i %	p kPa	u_w kPa	$p-u_w$ kPa	p^* kPa	q kPa	e	v 1+e	Sr (%)
C22(50)	21.82	21.82	74.8	-0.1	74.9	74.9	74.5	0.68	1.68	86.44
C22(150)	22.16	22.16	180.9	86.8	94.1	110.3	92.7	0.71	1.71	81.34
C22(300)	22.01	22.01	340.9	208.6	132.3	158.6	123.0	0.68	1.68	87.39
D22-20(150) 1	21.92	19.78	216.0	-0.7	216.7	216.6	197.8	0.60	1.60	88.68
D22-20(150) 2	22.09	20.08	215.9	-0.2	216.1	216.1	198.1	0.66	1.66	82.19
D22-19(150)	21.37	19.04	218.7	-0.1	218.8	218.8	205.7	0.62	1.62	82.42
D22-16(50)	21.45	16.84	179.8	-276.3	456.1	430.6	389.2	0.50	1.50	90.77
D22-16(300)	21.00	15.8	466.7	-142.4	609.1	586.5	499.8	0.51	1.51	84.13
D22-14(150)	21.74	13.97	325.0	-290.8	615.9	541.1	525.0	0.51	1.51	74.32

Figure 26 presents the Critical State points over the stress plane ($q–p-u_w$ plane). A regression analysis was carried out on the Critical State points for each group of tests at similar compaction water content. The resulting M values were: 0.84, 0.86 and 0.85 for samples that $w_{(ac)}$ were at 15%, 20% and 22% water content, respectively. The CSL of the CD tests is also shown in the figure.

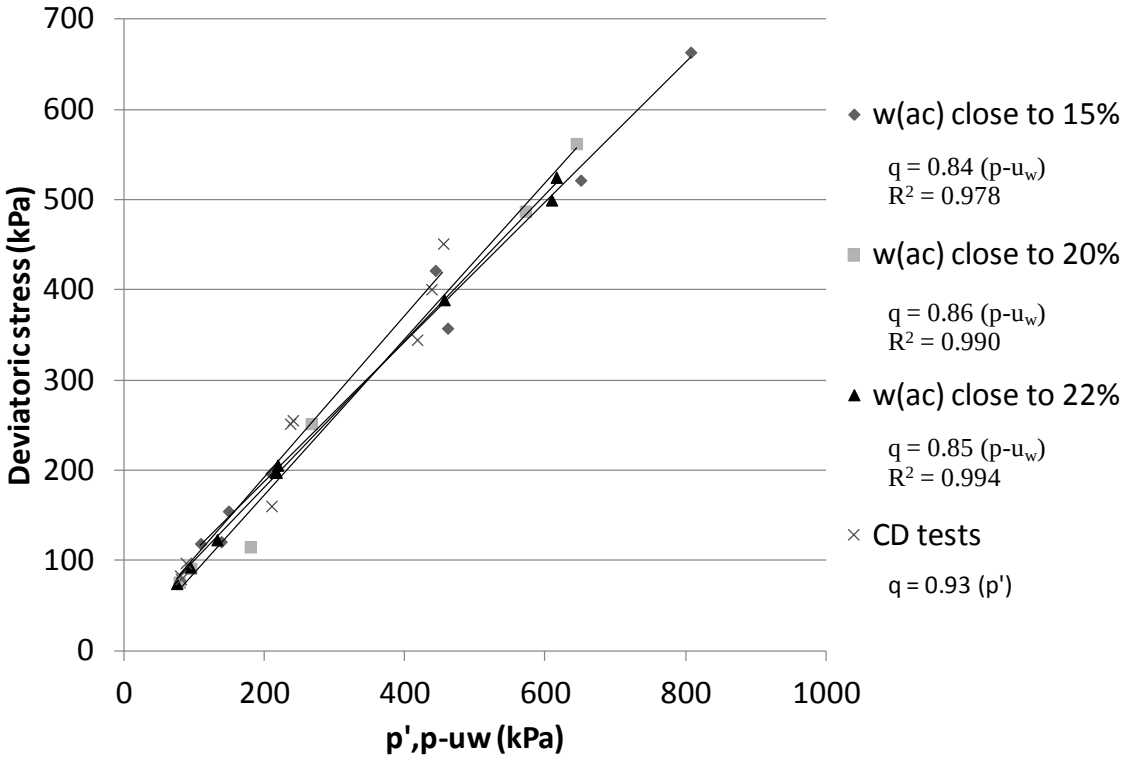

Figure 26 – Critical State Line of the CWC tests by $w_{(ac)}$ including the CD test series on q-(p-u_w) plane.

Table 8 presents a summary of the critical state line parameters determined from the constant water content and saturated tests. In the stress plane (q-p-u_w) similar M values were obtained for the constant water tests, giving similar critical state friction angles (ϕ'_{cv}) of 22°. These are a little lower than the effective stress friction angle of 24 ° obtained from the saturated tests. The reason for this will be explored later when interpreting the data in terms of Bishop stress, p*.

Table 8 – Critical State Line parameters of CD and CWC tests including the resulting friction angle.

	v – (p-u_w) plane		**q – (p-u_w) plane**	
	Γ	**λ**	**M**	**ϕ'_c**
CD tests	1.87	0.06	0.93	24°
CWC tests with $w_{(ac)}$ close to 22%	2.16	0.10	0.85	22°
CWC tests with $w_{(ac)}$ close to 20%	2.06	0.09	0.86	22°
CWC tests with $w_{(ac)}$ close to 15%	2.05	0.09	0.84	22°

Figure 27 presents the critical state points achieved by each constant water content test in the v–p-u_w space, identified by water content at compaction. A linear regression through the critical state points gave the slope of the critical state lines on the v–p-u_w space (λ) as being 0.09 for samples that had $w_{(ac)}$ close to 15%and 20% and 0.10 for samples that had $w_{(ac)}$ close to 22%. The critical state line for CD tests is also shown in the figure for reference.

In Figure 27, samples that were tested with a $w_{(ac)}$ closer to 22% presented higher values in the v–p-u_w plane, explained by a lower degree of saturation in samples compacted at this water content (81-87%) when compared with samples wetted to this water content from the 15% compaction conditions (91%) and 20% compaction conditions (84-91%).

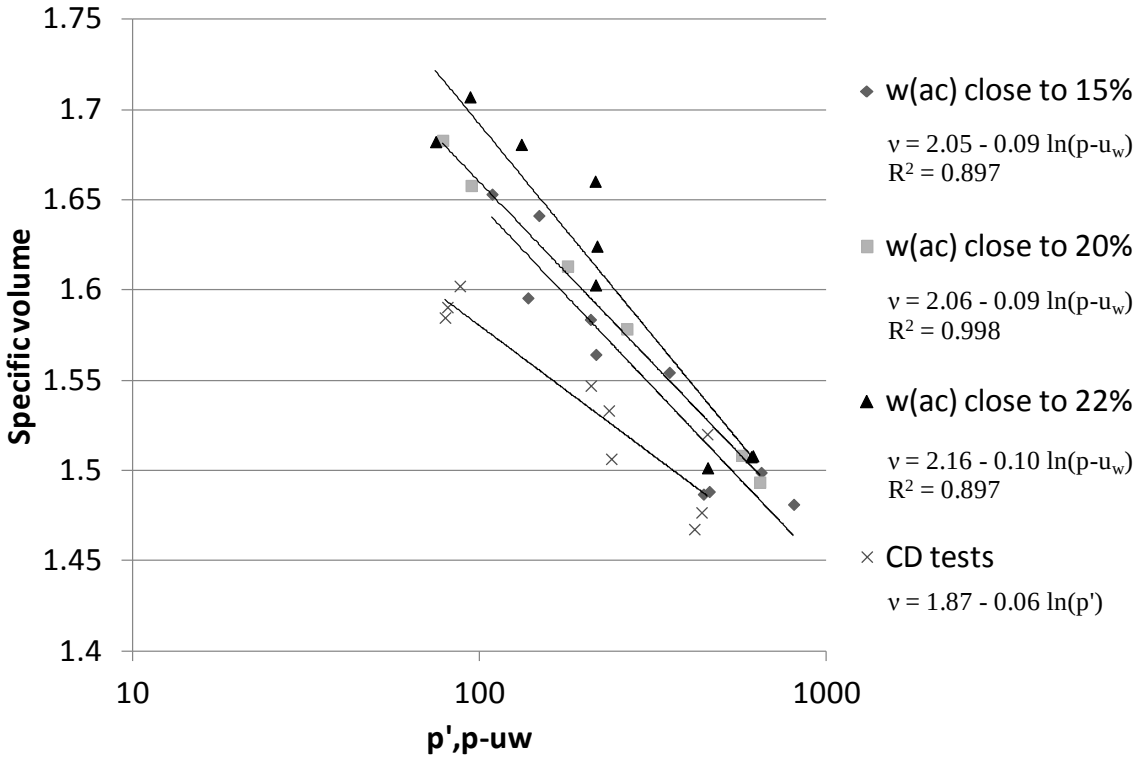

Figure 27 – Critical State Line of the CWC tests by $w_{(ac)}$ including the CD test series on v-p-u_w plane.

It can been seen from the summary of values in Table 8 that the slope of critical state lines in the v-p-u_w plane (λ) for the constant water content tests seem to be similar in value, however the intercept of the critical state line in v axis (Γ) increases with the increase of the $w_{(ac)}$ tested.

A different approach for the analysis of the critical state is to use the average skeleton stress assumption (Bishop stress) which incorporates the degree of saturation as shown in Eq. 2. From the critical state points obtained in Tables 5 to 7 the critical state lines in the q-p* plane were generated, Figure 28, and the v–p* plane, Figure 29. As is shown in Figure 28, by incorporating the degree of saturation, all the critical state points (saturated and unsaturated) fit on a single regression line. The slope of the critical state line in the stress plane (q-p* plane) was found to be M=0.91, resulting in a critical state friction angle (ϕ'_{cv}) of 23°.

The fact that the Bishop stress approach gives a consistent picture of shear strength for this data set is due to the fact that the degree of saturation is relatively high (generally >80%). It can be seen from the data for χ reported by Bishop and Blight (1963) that for high degrees of saturation, χ≅Sr. Bishop and Blight also noted that the interpretation of shear strength in terms of "effective stress" was less sensitive to stress and suction paths followed, and the data set reported here would corroborate that. Tarantino and Tombolato (2005) found that the Bishop stress approach was not sufficient to explain their data set on compacted kaolin, but this included data for degrees of saturation below 50%. Therefore, it can be concluded that the Bishop stress approach can provide a simple interpretation of shear strength data for high degrees of saturation only (>80%).

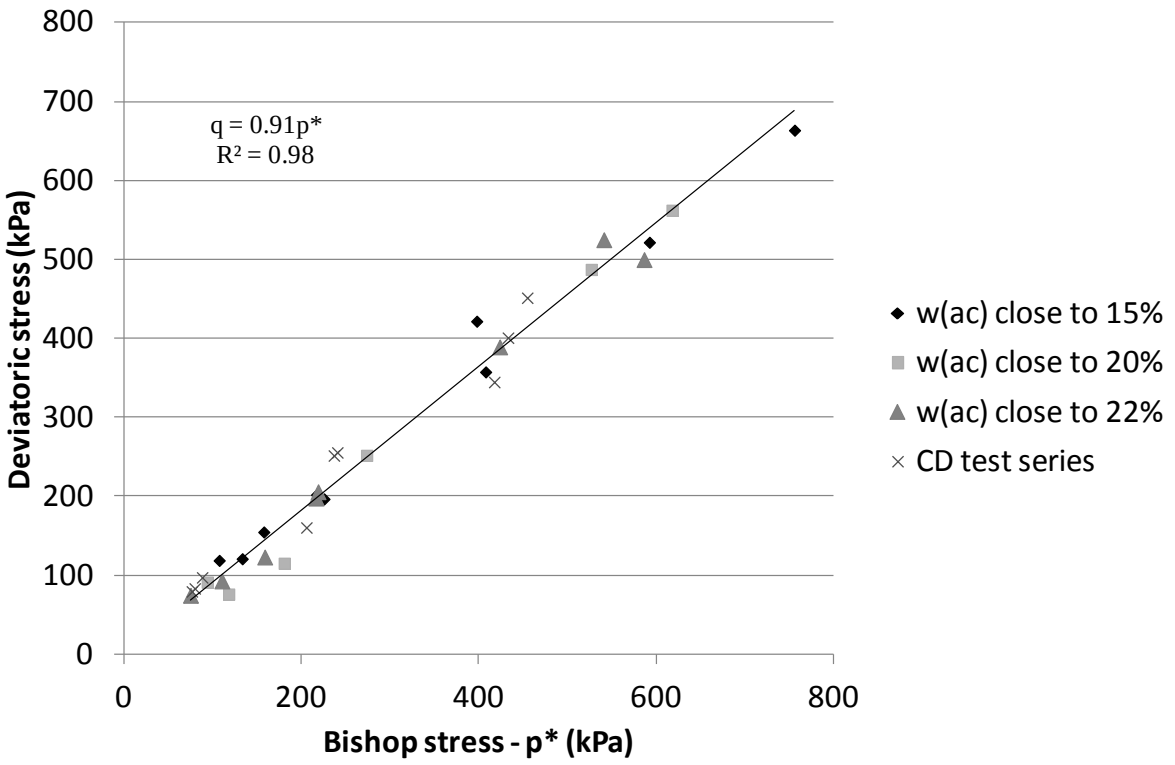

Figure 28 - Critical State Line of the CWC tests by $w_{(ac)}$ including the CD test series on p*-q plane.

Bishop stress has also been used to consider the volumetric behaviour and the data is presented in the ν–p* plane in Figure 29. It can be seen that different regressions for the critical state points for different $w_{(ac)}$ were obtained, as was also seen in the ν–p-u_w plane in Figure 27. This time, for the CWC tests interpreted in terms of Bishop stress, λ increased with as-compacted water content ($w_{(ac)}$) ranging 0.11 for samples with $w_{(ac)}$ close to 22%, 0.10 for samples with $w_{(ac)}$ close to 20% and 0.09 for samples with $w_{(ac)}$ close to 15%.

Table 9 summarises the critical state parameters obtained using the average skeleton (Bishop) stress. Although a better fitting of the critical state points was achieved in the stress plane, on the volumetric plane different parameters were obtained for different compaction water contents. This demonstrates clearly that a simple "effective stress" approach cannot, by itself, explain the volumetric behaviour. This is consistent with Bishop and Blight's (1963) observations of difficulties in interpreting stress-volume change relationships. It indicates the importance of the initial compacted fabric, which in unsaturated soils is not destroyed by shearing, as suction is able to support and maintain the aggregated double structure of compacted unsaturated soils (Toll, 1990; Toll, 2000; Toll and Ong, 2003).

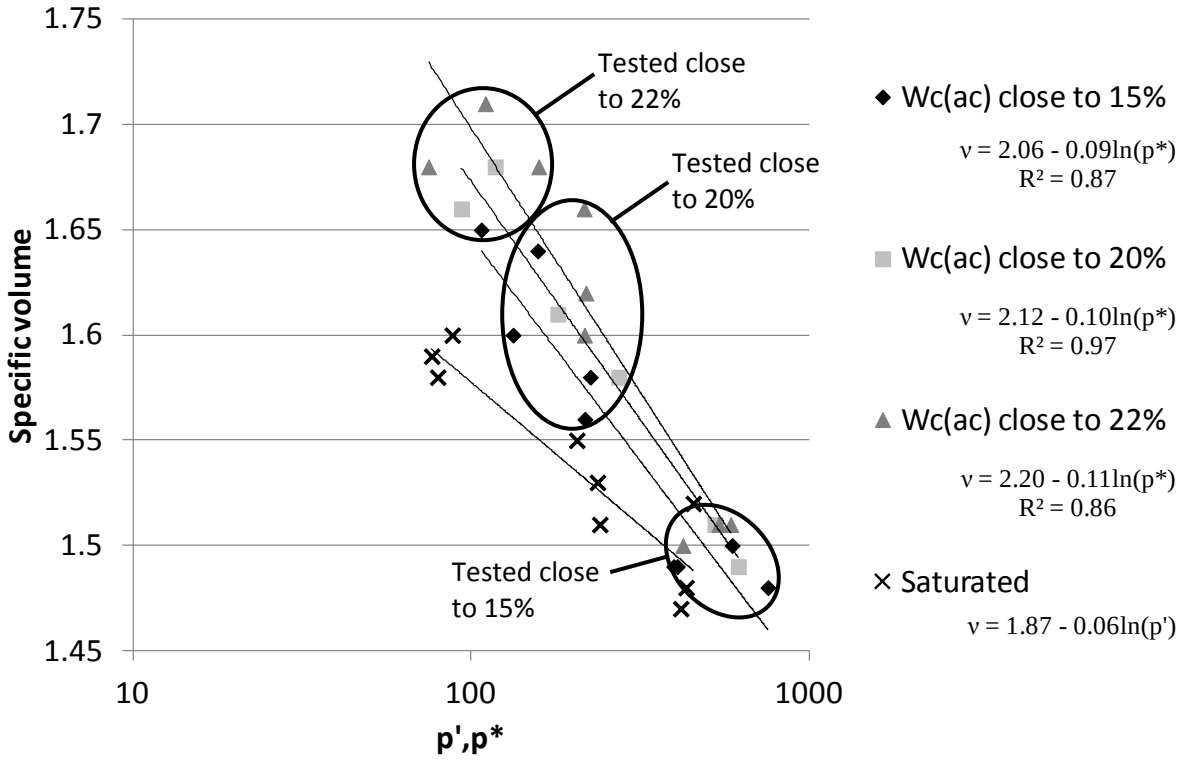

Figure 29 - Critical State Line of the CWC tests by $w_{(ac)}$ including the CD test series on ν-p* plane.

Table 9 - Critical state line parameters of CD and CWC tests including the resulting friction angle using Bishop average skeleton stress.

	ν – p* plane **ν – p' plane**		**q – p* plane** **q – p' plane**	
	Γ	**λ**	**M**	**∅'**
CD tests	1.87	0.06	0.91	23^0
CWC tests with $w_{(ac)}$ close to 22%	2.20	0.11		
CWC tests with $w_{(ac)}$ close to 20%	2.12	0.10		
CWC tests with $w_{(ac)}$ close to 15%	2.06	0.09		

The implication of this can be seen from Figure 29. If the tests sheared at the same water content are considered (shown grouped in Figure 29), there is a tendency for the samples compacted at the higher water content to plot on the high side of each data set and the tests that were compacted at a lower water content to plot on the low side. So, for the data set tested at 22% water content, the samples compacted at that water content (22%) plot highest; samples that have been wetted from 20% water content plot slightly lower and the sample wetted from 15% plots lower still. Similarly for the data set sheared at 20%. The sample compacted at that water content (20%) plots in the centre of the data set. Samples dried back from 22% plot at a slightly higher level and samples wetted up from 15% plot at a lower level. For the samples sheared at 15%, the samples compacted at that water content (15%) tend to plot lowest, while samples dried back from 20% and 22% plot above.

An example of what this means in terms of strength can be seen in Figure 30, where the stress paths (in terms of Bishop stress) are plotted for specimens sheared at close to 20% water content. By comparing two tests at a confining stress of 300kPa, it can be seen that the sample compacted at 20% (C20(300)) reaches the Critical State Line at q= 252 kPa. However, the sample wetted from 15% (W15-19(300)) reaches the Critical State Line at q =197 kPa. This means a 20% reduction in strength for the wetted sample compared to the as compacted condition, even though the water content at shearing is slightly lower. Similarly, if samples tested at 150 kPa confining stress are compared, samples that are dried to that water content (D22-20(150) 1; D22-20(150) 2 and D22-19(150) all

reach the Critical State Line at around q=200 kPa. However, a sample wetted to that water content (W15-20(150)) reaches the Critical state line at around q = 155 kPa.

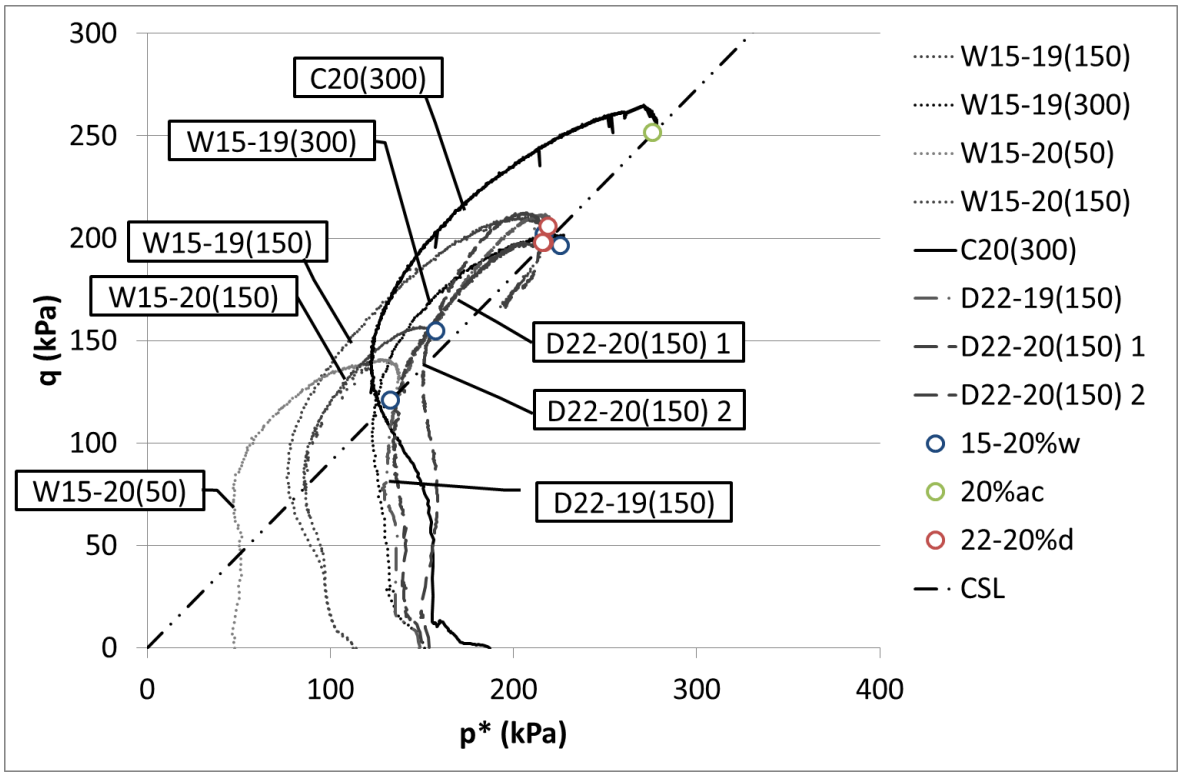

Figure 30 – Stress paths (in terms of Bishop stress) for samples tested close to 20% water content .

Therefore, from the analysis performed using a Critical State approach, it could be determined that the mechanical behaviour of the fill material at Critical State is governed by the initial water content; the as-compacted condition of the samples is seen to have an influence on the volumetric behaviour of the material. Although the critical state stress ratio, M, itself is not affected by the initial water content, the position at which the stress path reaches the Critical State Line is affected by the subsequent processes of wetting and drying. This means that samples that are dried back to a particular water content have a higher strength than a sample compacted at that water content; conversely, a sample wetted to achieve that water content have a lower strength.

8 Conclusions

A testing program involving a series of constant water content triaxial tests on unsaturated samples, backed up by a series of consolidated drained tests on saturated samples, was carried out in an attempt to describe the mechanical behaviour of a sandy clay soil. While the saturated tests were performed in conventional triaxial cells, the constant water content tests were performed in double cell triaxial cells. Constant water tests were carried out on samples at pre-determined water contents (15%, 20% and 22%). From these starting water contents samples were tested under dried, wetted or as-compacted conditions. Testing was carried out at different confining pressures (50, 150 and 300kPa).

Sets of critical state parameters were determined from the triaxial tests for each starting water content, where similarities in v-(p-u_w) plane and the q–(p-u_w) were obtained. The slope of the Critical State line in the v-(p-u_w) plane (λ) and slope of critical state line on the q-p-u_w plane (M) did not differ much from the different water contents tested, 0.09, 0.09 and 0.10 for λ and 0.84, 0.86 and

0.85 for M, for $w_{(ac)}$ close to 15%, 20% and 22% respectively. Only the intercept of the critical state line in v axis (Γ) differed, increasing with an increase in water content (at compaction), 2.05 ($w_{(ac)}$ close to 15%) to 2.06 ($w_{(ac)}$ close to 20%) to 2.16 ($w_{(ac)}$ close to 22%).

With an approach using Bishop average skeleton stress (p*) a better fitting was achieved in the stress plane. The M value for unsaturated tests changed from 0.84-0.86 to values of 0.9-0.91, resulting in a better fit with data obtained from the saturated tests of 0.93. This suggests that the Bishop stress approach can provide a simple interpretation of shear strength data for high degrees of saturation (>80%). However, in the v–p* plane, different critical state lines were obtained for different as-compacted water contents. This indicates the importance of the initial compacted fabric, which in unsaturated soils is not destroyed by shearing, as suction is able to support and maintain the aggregated double structure of compacted unsaturated soils.

The mechanical behaviour of the fill material was found to be affected by the initial conditions, the as-compacted conditions. Although the critical state stress ratio, M, itself was not affected by the initial water content, the differences in volumetric behaviour did lead to differences for samples subjected to wetting and drying after compaction. Samples that were dried back to a particular water content had a higher strength than samples compacted at that water content; conversely, a samples wetted to achieve that water content had a lower strength.

Acknowledgements

The testing work described in this paper was funded by the Engineering and Physical Sciences Research Council, Grant GR/S87430/01 *Biological and Engineering Impacts of Climate Change on Slopes (BIONICS)* and subsequent analysis has been supported by Grant EP/K027050/1 *Infrastructure Slopes: Sustainable Management and Resilience Assessment (iSmart).*

References

Bishop A.W. (1959). *The Principle of Effective Stress*, Tecknisk Ukeblad, 106, 39, pp. 859-863.

Bishop, A.W., Alpan, I., Blight, G.E. and Donald, I.B. (1960) *Factors controlling the strength of partly saturated cohesive soils*. Proc. ASCE Reasearch Conf. on Shear Strength of Cohesive Soils, Boulder, Colorado, USA, pp. 503-532.

British Standard Institute (1990), BS1377: *Methods of test for Soils of civil engineering purposes*, *BSI*, Milton Keynes.

Escario, V. & Saez, J. (1986). *The shear strength of partly saturated soils*. Géotechnique 36, No. 3, pp. 453-456.

Fredlund D. G. and Morgenstern N. R. (1977), *Stress state variables for unsaturated soils*. *J. Geotech. Eng. Div., ASCE* **103**, GT5, pp. 447-466.

Fredlund, D.G, Morgenstern, N.R., and Widger, R.A. (1978) *The Shear Strength of Unsaturated Soils*. Canadian Geotechnical Journal 15, pp. 313-321.Hughes, P.N., Glendinning, S. and Mendes, J. (2007). *Construction Testing and Instrumentation of an infrastructure testing embankment,* Proc. Expert Symposium on Climate Change: Modelling, Impacts and Adaptations, Singapore, pp. 159-166.

Hughes, P.N., Glendinning, S., Mendes, J., Parkin, G., Toll, D.G., Gallipoli, D., Miller, P. (2009). *Full-scale testing to assess climate effects on embankments*. Special Issue of Engineering Sustainability: Proc. Institution of Civil Engineers, 162(2), pp. 67-79.

Jenkins, G., Murphy, J., Sexton, D., Lowe, J., Jones, P. and Kilsby, C. (2010), *Climate Projections: Briefing Report*, www.UKclimateprojections.defra.gov.uk

Jommi, C. (2000), *Remarks on the constitutive modelling of unsaturated soils,* Experimental Evidence and Theoretical Approaches in Unsaturated Soils, Tarantino & Mancuso (eds), Balkema, Rotterdam, pp. 139-153.

Khalili, N. and Khabbaz, M.H. (1998) *A Unique Relationship for chi for the determination of the Shear Strength of Unsaturated Soils,* Géotechnique, Vol. 48(5), pp. 681-687.

Lourenço, S.D.N., Gallipoli, D., Toll, D.G. and Evans, F.D. (2006) *Development of a Commercial Tensiometer for Triaxial Testing of Unsaturated Soils*, Proc. 4th International Conference on Unsaturated Soils, Phoenix, USA, Geotechnical Special Publication No. 147, Reston: ASCE, Vol.2, pp. 1875-1886.

Lourenço, S.D.N., Gallipoli, D., Toll, D.G., Augarde, C.E. and Evans, F.D. (2011) *Towards a tensiometer based suction control system for laboratory testing of unsaturated soils*, ASTM Geotechnical Testing Journal, 34(6), pp. 755-764.

Mendes, J. (2011), *Assessment of the Impact of Climate Change on an Instrumented Embankment: An unsaturated soil mechanics approach*. PhD thesis, Durham University.

Mendes, J, Toll, D.G. and Evans, F. (2012), *A Double Cell Triaxial System for Unsaturated Soils Testing*, in Mancuso, C., Jommi, C. & D'Onza F. eds, Unsaturated Soils: Research and Applications **1**: 2nd European Conference on Unsaturated Soils. Naples, Italy, Springer, pp. 5-10.

Tarantino, A. and Tombolato, S. (2005), *Coupling of hydraulic and mechanical behaviour in unsaturated compacted clay*. Géotechnique 55(4), pp. 307–317.

Toll, D.G. (1990), A framework for unsaturated soil behaviour. Geotechnique, 40(1), pp. 31-44.

Toll, D.G.(1999), *A Data acquisition and control system for geotechnical testing*. Computing developments in civil and structural engineering (eds. B. Kumar and B.H.V. Topping), Edinburgh: Civil-Comp Press, pp 237-242.

Toll, D.G. (2000) *The Influence of Fabric on the Shear Behaviour of Unsaturated Compacted Soils*, in Advances in Unsaturated Soils (eds. C. Shackleford, S.L. Houston and N-Y. Chang) Geotechnical Special Publication No. 99, Reston: American Society of Civil Engineers, pp 222-234.

Toll, D.G. and Ong. B.H. (2003) *Critical State Parameters for an Unsaturated Residual Sandy Clay*, Géotechnique, Vol. 53(1), pp 93-103.

Wheeler, S. J. and Sivakumar, V. (1995), *An elasto-plastic critical state framework for unsaturated soil*. Géotechnique 45(1), pp 35–53.

Wheeler, S. J. and Sivakumar, V. (2000), *Influence of compaction procedure on the mechanical behaviour of an unsaturated compacted clay. Part 2: Shearing and constitutive modelling*. Géotechnique 50(4), pp 369–376.